Inorganic Chemistry

Article

pubs.acs.org/IC

Reactivity of Biomimetic Iron(II)-2-aminophenolate Complexes toward Dioxygen: Mechanistic Investigations on the Oxidative C−C Bond Cleavage of Substituted 2-Aminophenols§

Biswarup Chakraborty,† Sourav Bhunya,‡ Ankan Paul,‡ and Tapan Kanti Paine*,†

†Department of Inorganic Chemistry, ‡Raman Center for Atomic, Molecular and Optical Sciences, Indian Association for the Cultivation of Science, 2A & 2B Raja S. C. Mullick Road, Jadavpur, Kolkata 700032, India

Supporting Information

ABSTRACT: The isolation and characterization of a series of iron(II)-2-aminophenolate complexes $[(6\text{-}Me_3\text{-}TPA)Fe^{II}(X)]^+$ (X = 2-amino-4-nitrophenolate (4-NO_2-HAP), **1**; X = 2-aminophenolate (2-HAP), **2**; X = 2-amino-3-methylphenolate (3-Me-HAP), **3**; X = 2-amino-4-methylphenolate (4-Me-HAP), **4**; X = 2-amino-5-methylphenolate (5-Me-HAP), **5**; X = 2-amino-4-*tert*-butylphenolate (4-^{t}Bu-HAP), **6** and X = 2-amino-4,6-di-*tert*-butylphenolate (4,6-di-^{t}Bu-HAP), **7**) and an iron(III)-2-amidophenolate complex $[(6\text{-}Me_3\text{-}TPA)Fe^{III}(4,6\text{-di-}^t\text{Bu-AP})]^+$ ($\mathbf{7^{Ox}}$) supported by a tripodal nitrogen ligand (6-Me_3-TPA = tris(6-methyl-2-pyridylmethyl)amine) are reported. Substituted 2-aminophenols were used to prepare the biomimetic iron(II) complexes to understand the effect of electronic and structural properties of aminophenolate rings on the dioxygen reactivity and on the selectivity of C−C bond cleavage reactions. Crystal structures of the cationic parts of **5**·ClO_4 and **7**·BPh_4 show six-coordinate iron(II) centers ligated by a neutral tetradentate ligand and a monoanionic 2-aminophenolate in a bidentate fashion. While **1**·BPh_4 does not react with oxygen, other complexes undergo oxidative transformation in the presence of dioxygen. The reaction of **2**·ClO_4 with dioxygen affords 2-amino-3*H*-phenoxazin-3-one, an auto-oxidation product of 2-aminophenol, whereas complexes **3**·BPh_4, **4**·BPh_4, **5**·ClO_4 and **6**·ClO_4 react with O_2 to exhibit C−C bond cleavage of the bound aminophenolates. Complexes **7**·ClO_4 and $\mathbf{7^{Ox}}$·BPh_4 produce a mixture of 4,6-di-*tert*-butyl-2*H*-pyran-2-imine and 4,6-di-*tert*-butyl-2-picolinic acid. Labeling experiments with $^{18}O_2$ show the incorporation of one oxygen atom from dioxygen into the cleavage products. The reactivity (and stability) of the intermediate, which directs the course of aromatic ring cleavage reaction, is found to be dependent on the nature of ring substituent. The presence of two *tert*-butyl groups on the aminophenolate ring in **7**·ClO_4 makes the complex slow to cleave the C−C bond of 4,6-di-^{t}Bu-HAP, whereas **4**·BPh_4 containing 4-Me-HAP displays fastest reactivity. Density functional theory calculations were conducted on $[(6\text{-}Me_3\text{-}TPA)Fe^{III}(4\text{-}^t\text{Bu-AP})]^+$ ($\mathbf{6^{Ox}}$) to gain a mechanistic insight into the regioselective C−C bond cleavage reaction. On the basis of the experimental and computational studies, an iron(II)-2-iminobenzosemiquinonate intermediate is proposed to react with dioxygen resulting in the oxidative C−C bond cleavage of the coordinated 2-aminophenolates.

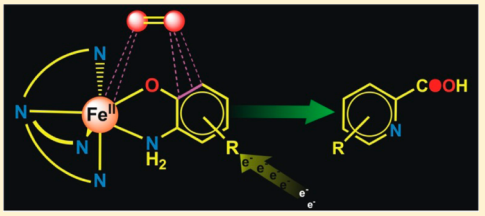

INTRODUCTION

Aromatic C−C bond cleavage is a crucial step in the biodegradation of organic compounds such as catechols, aminophenols, hydroquinones, salicylic acid, gentisic acid, etc. by aerobic microorganism.[1−7] A variety of nonheme iron oxygenases are involved in catalyzing the C−C bond cleavage of aromatic compounds in the biodegradation pathway.[8−17] Catechol dioxygenases are most familiar in this class of enzymes which is categorized as extradiol and intradiol dioxygenases depending upon the position of ring cleavage of catechol.[9,18−20] 2-Aminophenol dioxygenases catalyze the ring cleavage at meta position of 2-aminophenols in the biodegradation of nitroaromatics.[21−23] 2-Aminophenol-1,6-dioxygenase (APD), the nonheme iron enzyme isolated and purified from *Pseudomonas pseudoalcaligenes*, catalyzes the oxygenolytic ring cleavage of 2-aminophenols under aerobic conditions.[11,24,25] The reaction occurs via oxidative C1−C6 bond cleavage to form 2-aminomuconic acid semialdehyde which spontaneously cyclizes with loss of a water molecule to form 2-picolinic acid (Scheme 1). Very recently, the crystal structures of APD from *Comamonas* sp. strain CNB-1 as the apoenzyme, the holoenzyme and as complexes with the lactone intermediate (4*Z*,6*Z*)-3-iminooxepin-2(3*H*)-one, and the product 2-aminomuconic acid-6-semialdehyde with the suicide inhibitor 4-nitrocatechol have been reported.[26] The active site structure in the resting state shows the binding of aminophenolate to the

Scheme 1. Reaction Catalyzed by 2-Aminophenol Dioxygenases

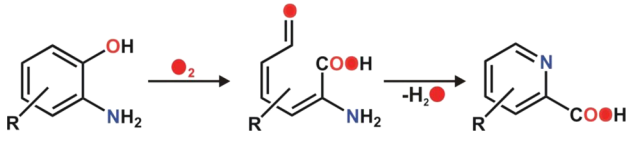

Received: December 11, 2013
Published: May 1, 2014

   dx.doi.org/10.1021/ic403043e | *Inorg. Chem.* 2014, 53, 4899−4912

ferrous ion and the other structures provide insight into the reaction mechanism. Another related enzyme, 3-hydroxyanthranilate-3,4-dioxygenase (HAD), isolated from *Saccharomyces cerevisiae*, catalyzes the C3−C4 bond cleavage of 3-hydroxyanthranilate to quinolinic acid in the tryptophan catabolism pathway.[27−30] A similar pathway is followed in the degradation of other nitroaromatic compounds.[25,31−34] Both HAD and APD exhibit a common "2-His-1-carboxylate" structural motif and show functional similarity with extradiol dioxygenases.

On the basis of structural and biochemical studies on HAD and APD, a mechanistic proposal similar to that of extradiol catechol dioxygenases has been reported (Scheme 2).[29,30] The

Scheme 2. Proposed Catalytic Cycle of 2-Aminophenol Dioxygenases

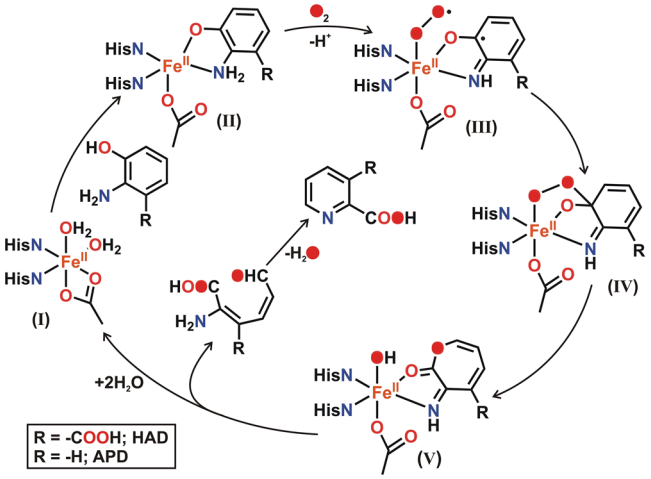

substrate binds to the ferrous ion and the enzyme−substrate complex (**II**) activates dioxygen. An iron(II)-peroxide intermediate (**IV**) is subsequently generated via an iron(II)-2-iminobenzosemiquiononate species (**III**) upon electron transfer from the aminophenolate ring to the metal center. A lactone intermediate (**V**) is formed via Criegee rearrangement of the iron(II)-peroxide intermediate (**IV**) with the incorporation of one oxygen atom into the lactone ring. Hydrolysis of the lactone affords the cleavage product. The conversion of 2-amino muconic acid semialdehyde to 2-picolinic acid then takes place through a nonenzymatic pathway.[33] Most of the intermediates have been successfully characterized crystallographically in APD similar to the structures isolated with different enzyme stains of homoprotocatechuate 2,3-dioxygenase (HPCD).[26,35]

The ring cleavage reactivity of 2-aminophenol dioxygenases (HAD and APD) has fuelled the interest in studying the reactivity of iron-coordinated 2-aminophenols. The "redox non-innocent" nature of aminophenols (Scheme 3) is the key electronic feature responsible for dioxygen activation and subsequent aromatic C−C bond cleavage reaction catalyzed by

Scheme 3. Redox Non-innocence of 2-Aminophenolates

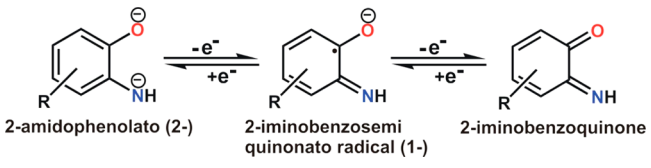

the enzymes. Wieghardt and Chaudhuri reported a number of metal complexes where the coordinated aminophenolates exhibited different oxidation states.[36−42] Fiedler and co-workers have recently reported an iron(II)-2-aminophenolate complex with a facial N_3 donor ligand. Reaction of the iron(II) complex with an oxidant led to the isolation of an iron(II)-2-iminobenzosemiquinonate and iron(III)-2-iminobenzosemiquinone complexes.[43,44] In biomimetic chemistry, reactivity of model iron(II)-aminophenolate is less explored. Recently, we have reported a six-coordinate iron(II)-aminophenolate complex of a tetradentate ligand, $[(6\text{-Me}_3\text{-TPA})\text{Fe}^{\text{II}}(4\text{-}^t\text{Bu-HAP})]^+$ (6-Me_3-TPA = tris(6-methyl-2-pyridylmethyl)amine), as the first functional model of 2-aminophenol dioxygenases.[45] The complex reacts with dioxygen under ambient conditions to undergo oxidative C−C bond cleavage of 2-amino-4-*tert*-butylphenol resulting in the formation of 4-*tert*-butyl-2-picolinic acid as the only product.[45] In the model system, the iron(II)-aminophenolate complex initially reacts with O_2 to form the corresponding iron(III)-amidophenolate complex. For further understanding of the mechanism of C−C bond cleavage of 2-aminophenol on the iron(II) complex of N_4 ligand, we have studied the dioxygen reactivity of a series of iron(II)-2-aminophenolate complexes with different substituents on the aminophenolate ring. In this Article, we report the synthesis and characterization of six iron(II)-2-aminophenolate complexes with the general formula $[(6\text{-Me}_3\text{-TPA})\text{Fe}^{\text{II}}(\text{X})]^+$ (X = 2-amino-4-nitrophenolate (4-NO_2−HAP), 2-aminophenolate (HAP), 2-amino-3-methylphenolate (3-Me-HAP), 2-amino-4-methylphenolate (4-Me-HAP), 2-amino-5-methylphenolate (5-Me-HAP), and 2-amino-4,6-di-*tert*-butylphenolate (4,6-di-^{t}Bu-HAP)) (Scheme 4). The influence of structural and electronic properties of substituent on the dioxygen reactivity and on the oxidative C−C bond cleavage of aminophenols is discussed. On the basis of experimental and computational studies, a mechanism of the aromatic C−C bond cleavage reaction of substituted 2-aminophenols on an iron complex is presented.

EXPERIMENTAL SECTION

Materials and Physical Measurements. All reagents and solvents were purchased from commercial sources and were used without further purification. Solvents were distilled and dried before use. Preparation and handling of air-sensitive materials were carried out under an inert atmosphere in a glovebox. Ligand 6-Me_3-TPA was prepared according to a literature procedure.[46] Fourier transform infrared spectroscopy (FT-IR) on KBr pellets was performed on a Shimadzu FT-IR 8400S instrument. Elemental analyses were performed on a PerkinElmer 2400 series II CHN analyzer. Electrospray ionization (ESI) mass spectra were recorded with a Waters QTOF Micro YA263 instrument. Solution electronic spectra (single and time-dependent) were measured on an Agilent 8453 diode array spectrophotometer. All room temperature NMR (Nuclear Magnetic Resonance) spectra were collected on a Bruker Avance 500 MHz spectrometer. Room temperature magnetic data were collected on Gouy balance (Sherwood Scientific, Cambridge, UK). Diamagnetic contributions were calculated for each compound using Pascal's constants. GC-MS (Gas Chromatography−Mass Spectrometry) measurements were carried out on a PerkinElmer Clarus 680 GC and SQ8T MS, using Elite 5 MS (30 m x 0.25 mm x 0.25 μm) column with maximum temperature of 300 °C. X-band EPR (Electron Paramagnetic Resonance) measurements were performed on a JEOL JES-FA 200 instrument. Labeling experiments were carried out with $^{18}O_2$ gas (99 atom %) or H_2O^{18} (98 atom %) purchased from Icon Services Inc., USA.

General Procedure for the Syntheses of Iron(II)-2-aminophenol Complexes. Iron(II) perchlorate hydrate (0.36 g, 1.00

dx.doi.org/10.1021/ic403043e | Inorg. Chem. 2014, 53, 4899−4912

Scheme 4. Synthesis of Iron(II)-2-aminophenolate Complexes

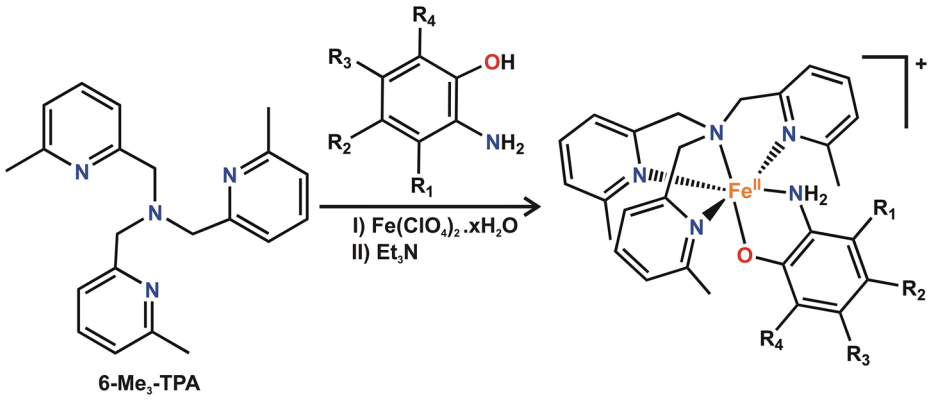

$R_1 = R_3 = R_4 = H$; $R_2 = NO_2$; $[(6\text{-}Me_3\text{-}TPA)Fe^{II}(4\text{-}NO_2\text{-}HAP)]^+$ **(1)**

$R_1 = R_2 = R_3 = R_4 = H$; $[(6\text{-}Me_3\text{-}TPA)Fe^{II}(HAP)]^+$ **(2)**

$R_2 = R_3 = R_4 = H$; $R_1 = CH_3$; $[(6\text{-}Me_3\text{-}TPA)Fe^{II}(3\text{-}Me\text{-}HAP)]^+$ **(3)**

$R_1 = R_3 = R_4 = H$; $R_2 = CH_3$; $[(6\text{-}Me_3\text{-}TPA)Fe^{II}(4\text{-}Me\text{-}HAP)]^+$ **(4)**

$R_1 = R_2 = R_4 = H$; $R_3 = CH_3$; $[(6\text{-}Me_3\text{-}TPA)Fe^{II}(5\text{-}Me\text{-}HAP)]^+$ **(5)**

$R_1 = R_3 = R_4 = H$; $R_2 =$ *tert*-butyl ; $[(6\text{-}Me_3\text{-}TPA)Fe^{II}(4\text{-}^t\text{Bu-}HAP)]^+$ **(6)**

$R_1 = R_3 = H$; $R_2 = R_4 =$ *tert*-butyl ; $[(6\text{-}Me_3\text{-}TPA)Fe^{II}(4,6\text{-di-}^t\text{Bu-}HAP)]^+$ **(7)**

mmol) was added to a solution of the ligand (1.00 mmol) in methanol (5 mL). To the resulting mixture was added a solution of aminophenol (1.00 mmol) and 1 equiv of Et_3N in methanol (5 mL). The solution was then allowed to stir at room temperature for 4 h. The solution was concentrated and diethyl ether was added. The resulting mixture was stirred further for 4−5 h to precipitate a solid. The solid was isolated by filtration, washed two to three times with diethyl ether and dried. Tetraphenylborate salts of the complexes were isolated from the reaction of the perchlorate salt with 1 equiv of sodium tetraphenylborate in methanol.

$[(6\text{-}Me_3\text{-}TPA)Fe^{II}(4\text{-}NO_2\text{-}HAP)](BPh_4)$ ***(1·BPh$_4$)***. Red solid. Yield: 0.61 g (71%). Anal. Calcd for $C_{51}H_{49}BFeN_6O_3$ (860.63 g/mol): C, 71.17; H, 5.74; N, 9.76. Found: C, 70.69; H, 5.61; N, 9.91%. IR (KBr, cm^{-1}): 3443(br), 3292(m), 3055(m), 1601(s), 1578(m), 1499(s), 1456(m), 1286(vs), 1086(m), 787(s), 735(s), 708(s). UV−vis in CH_3CN: 378 nm (ε = 16 000 $M^{-1}cm^{-1}$). Magnetic moment μ_{eff} (298 K): 4.8 μ_B. ^1H NMR (500 MHz, CD_3CN, 298 K): δ (ppm) 57.5 (6H) 46.7 (3H), 41.5 (3H), 31.3 (3H), 17.5 (1H), 16.3 (1H), 7.3 (8H), 6.9 (8H), 6.8 (4H), −33.2 (9H).

$[(6\text{-}Me_3\text{-}TPA)Fe^{II}(HAP)](ClO_4)$ ***(2·ClO$_4$)***. Yellow solid. Yield: 0.31 g (52%). Anal. Calcd for $C_{27}H_{30}ClFeN_5O_5$ (595.86 g/mol): C, 54.42; H, 5.07; N, 11.75. Found: C, 53.99; H, 4.84; N, 11.57%. IR (KBr, cm^{-1}): 3452(br), 3331(m), 1605(s), 1578(m), 1487(s), 1456(s), 1294(s), 1117(vs), 1094(vs), 781(m). UV−vis in CH_3CN: 401 nm (ε = 950 $M^{-1}cm^{-1}$). Magnetic moment μ_{eff} (298 K): 5.1 μ_B. ^1H NMR (500 MHz, $CDCl_3$, 298 K): δ (ppm) 51.9 (6H), 44.0 (3H), 37.3 (3H), 19.6 (3H), 7.4 (4H), −26.4 (9H).

$[(6\text{-}Me_3\text{-}TPA)Fe^{II}(3\text{-}Me\text{-}HAP)](BPh_4)$ ***(3·BPh$_4$)***. Yellow solid. Yield: 0.63 g (76%). Anal. Calcd for $C_{52}H_{52}BFeN_5O$ (829.66 g/mol): C, 75.28; H, 6.32; N, 8.44. Found: C, 75.31; H, 6.40; N, 8.27%. IR (KBr, cm^{-1}): 3431(br), 3055(m), 2926(m), 1605(s), 1578(s), 1466(vs), 1429(m), 1310(m), 785(m), 735(s), 706(vs). UV−vis in CH_3CN: 401 nm (ε = 1900 $M^{-1}cm^{-1}$). Magnetic moment μ_{eff} (298 K): 4.9 μ_B. ^1H NMR (500 MHz, $CDCl_3$, 298 K): δ (ppm) 43.9 (3H), 36.1 (3H), 19.6 (3H), 7.4 (3H), 7.3 (8H), 7.0 (8H), 6.7 (4H), −27.6 (9H).

$[(6\text{-}Me_3\text{-}TPA)Fe^{II}(4\text{-}Me\text{-}HAP)](ClO_4)$ ***(4·ClO$_4$)***. Yellow solid. Yield: 0.25 g (41%). Anal. Calcd for $C_{28}H_{32}ClFeN_5O_5$ (609.88 g/mol): C, 55.14; H, 5.29; N, 11.48. Found: C, 54.93; H, 5.22; N, 11.70%. IR (KBr, cm^{-1}): 3431(br), 3311(m), 2924(m), 1603(s), 1574(m), 1464(m), 1311(m), 1094(vs), 781(m), 625(s). UV−vis in CH_3CN: 403 nm (ε = 2110 $M^{-1}cm^{-1}$). Magnetic moment μ_{eff} (298 K): 4.9 μ_B.

$[(6\text{-}Me_3\text{-}TPA)Fe^{II}(4\text{-}Me\text{-}HAP)](BPh_4)$ ***(4·BPh$_4$)***. Yellow solid. Yield: 0.62 g (75%). Anal. Calcd for $C_{52}H_{52}BFeN_5O$ (829.66 g/mol): C, 75.28; H, 6.32; N, 8.44. Found: C, 74.78; H, 6.51; N, 8.35%. IR (KBr, cm^{-1}): 3431(br), 3053(m), 2922(m), 1605(s), 1578(m), 1491(vs), 1458(s), 1298(vs), 1010(w), 787(m), 739(s), 706(vs), 615. UV−vis in CH_3CN: 404 nm (ε = 2100 $M^{-1}cm^{-1}$). Magnetic moment μ_{eff} (298 K): 4.8 μ_B. ^1H NMR (500 MHz, $CDCl_3$, 298 K): δ (ppm) 52.9 (6H), 44.1 (3H), 38.2 (3H), 28.4 (3H), 19.0 (3H), 7.4 (3H), 7.3 (8H), 7.0 (8H), 6.7 (4H), −26.3 (9H).

$[(6\text{-}Me_3\text{-}TPA)Fe^{II}(5\text{-}Me\text{-}HAP)](ClO_4)$ ***(5·ClO$_4$)***. Yellow solid. Yield: 0.29 g (48%). Anal. Calcd for $C_{28}H_{32}ClFeN_5O_5$ (609.88 g/mol): C, 55.14; H, 5.29; N, 11.48. Found: C, 55.17; H, 5.18; N, 11.44%. IR (KBr, cm^{-1}): 3433(br), 3028(m), 2922(m), 1603(s), 1580(m), 1497(s), 1456(vs), 1302(s), 1157(m), 1120(vs), 1090(vs), 1009(m), 783(m), 627(m). UV−vis in CH_3CN: 401 nm (ε = 2200 $M^{-1}cm^{-1}$). Magnetic moment μ_{eff} (298 K): 5.1 μ_B. ^1H NMR (500 MHz, $CDCl_3$, 298 K): δ (ppm) 51.7 (3H), 43.9 (3H), 10.4 (3H), 7.4 (3H), −26.3 (9H).

$[(6\text{-}Me_3\text{-}TPA)Fe^{II}(4\text{-}^t\text{Bu-}HAP)](ClO_4)$ ***(6·ClO$_4$)***. The complex was synthesized according to the reported procedure.[45]

$[(6\text{-}Me_3\text{-}TPA)Fe^{II}(4,6\text{-di-}^t\text{Bu-}HAP)](ClO_4)$ ***(7·ClO$_4$)***. Yellow solid. Yield: 0.31 g (44%). Anal. Calcd for $C_{35}H_{46}ClFeN_5O_5$ (708.07 g/mol): C, 59.37; H, 6.55; N, 9.89. Found: C, 59.41; H, 6.58; N, 9.93%. IR (KBr, cm^{-1}): 3425(m), 2950(s), 2864(m), 1605(s), 1578(m), 1460(s), 1443(m), 1302(m), 1277(m), 1115(vs), 1094(vs), 789(m), 635(m). UV−vis in CH_3CN: 405 nm (ε = 2250 $M^{-1}cm^{-1}$) . Magnetic moment μ_{eff} (298 K): 5.2 μ_B.

$[(6\text{-}Me_3\text{-}TPA)Fe^{II}(4,6\text{-di-}^t\text{Bu-}HAP)](BPh_4)$ ***(7·BPh$_4$)***. Yellow solid. Yield: 0.62 g (67%). Anal. Calcd for $C_{59}H_{66}BFeN_5O$ (927.84 g/mol): C, 76.37; H, 7.17; N, 7.55. Found: C, 75.97; H, 7.21; N, 7.64%. IR (KBr, cm^{-1}): 3522(m), 3321(m), 3055(m), 2949(m), 1605(s), 1578(s), 1456(vs), 1302(s), 1277(m), 733(vs), 706(vs), 611(s). UV−vis in CH_3CN: 403 nm (ε = 2300 $M^{-1}cm^{-1}$). Magnetic moment μ_{eff} (298 K): 5.2 μ_B. ^1H NMR (500 MHz, $CDCl_3$, 298 K): δ (ppm) 53.6 (6H), 43.7 (3H), 37.3 (3H), 18.4 (3H), 7.4 (2H), 7.3 (8H), 7.0 (8H), 6.7 (4H), −25.9 (9H).

$[(6\text{-}Me_3\text{-}TPA)Fe^{III}(4,6\text{-di-}^t\text{Bu-}AP)](BPh_4)$ ***(7^{Ox}·BPh$_4$)***. Complex **7**·BPh_4 (37 mg, 0.04 mmol) was dissolved in dichloromethane (10

dx.doi.org/10.1021/ic403043e | Inorg. Chem. 2014, 53, 4899−4912

mL). To the solution was added $KMnO_4$ (6.3 mg, 0.04 mmol) or 2,4,6-tri-*tert*-butylphenoxy radical (10.4 mg, 0.04 mmol). The reaction mixture was stirred for 3 h and filtered to remove the solid particles. The filtrate was then concentrated to dryness and the residue was washed thoroughly with diethyl ether for two to three times. The dark green solid was then isolated by filtration and dried under vacuum. Yield: 23 mg (62%). Anal. Calcd for $C_{59}H_{65}BFeN_5O$ (926.84 g/mol): C, 76.46; H, 7.07; N, 7.56. Found: C, 76.61; H, 7.13; N, 7.66%. IR (KBr, cm^{-1}): 3435(br), 3053(m), 2957(s), 1605(s), 1578(s), 1460(vs), 1300(m), 1271(m), 787(m), 735(s), 706(vs), 611(s). UV−vis in CH_3CN: 366 nm (ε = 3000 cm^{-1} M^{-1}), 618 nm (ε = 1900 cm^{-1} M^{-1}), and 925 nm (ε = 2700 cm^{-1} M^{-1}).

Reaction of the Complexes with Dioxygen and Analysis of Organic Products. In a typical reaction, dry oxygen gas was bubbled through a solution of iron(II)-aminophenol complex (0.02 mmol) in dry acetonitrile (10 mL) for 2 min. The solution was kept for stirring at room temperature under oxygen environment. The yellow solution immediately turned deep green and then slowly to orange. The solvent was evaporated to dryness and the residue was treated with 2 *M* HCl solution (10 mL) to maintain the pH between 2 and 3. The organic products were then extracted with diethyl ether (3 × 15 mL), the combined organic layer was washed with a saturated brine solution, and dried over anhydrous Na_2SO_4. After removal of the solvent the solid mass was analyzed by ^1H NMR and GC-MS without further purification.

To identify the organic products, ^1H NMR spectra were compared with that of the commercially available standards (2-picolinic acid) or previously reported similar compounds (4-*tert*-butyl-2-picolinic acid and 4,6-di-*tert*-butyl-2-pyrone).[45,47] Quantification of organic product was performed by ^1H NMR spectroscopy with respect to the sharp singlet resonance at 6.8 ppm for four aromatic protons of *p*-benzoquinone standard.

^1H NMR (500 MHz, $CDCl_3$, 298 K): 3-Methyl-2-picolinic acid: δ (ppm) 8.49 (d, 1H, *J* = 4 Hz), 7.95 (d, 1H, *J* = 4 Hz), 7.46 (t, 1H, *J* = 5 Hz), 2.12 (s, 3H). 4-Methyl-2-picolinic acid: δ (ppm) 8.60 (d, 1H, *J* = 4 Hz), 7.98 (s, 1H), 7.53 (d, 1H, *J* = 5 Hz), 1.66 (s, 3H). 5-Methyl-2-picolinic acid: δ (ppm) 8.57 (s, 1H), 8.04 (d, 1H, *J* = 6 Hz), 7.64 (d, 1H, *J* = 5 Hz), 1.67 (s, 3H). 4,6-Di-*tert*-butyl-2-picolinic acid: δ(ppm) 8.07 (s, 1H), 7.59 (s, 1H), 1.27 (s, 9H), 1.40 (s, 9H). 4,6-Di-*tert*-butylpyran-2-imine: δ (ppm) 6.05 (s, 1H), 1.21 (s, 9H), 1.36 (s, 9H).

A control experiment with iron(II) perchlorate hydrate and sodium 2-amino-4,6-di-*tert*-butylphenolate (0.02 mmol) in acetonitrile solution under oxygen environment was performed to understand the role of the ligand and to ensure that no residual aminophenolate was present in the aqueous part after acidic work-up. After stirring the reaction mixture for 24 h under oxygen atmosphere, the solution was evaporated to dryness. The residue was treated with 2 *M* HCl solution (10 mL) to maintain the pH in the range of 2−3. The solution was then extracted with diethyl ether (3 × 15 mL) and the organic layer was dried over anhydrous Na_2SO_4. Analyses of organic species by ^1H NMR spectroscopy revealed quantitative isolation of 2-amino-4,6-di-*tert*-butylphenol without any C−C bond cleavage.

Methyl-4,6-di-tert-butyl-2-picolinate. The organic product, isolated from the reaction solution according to the procedure mentioned above, was reacted with excess diazomethane in dry diethyl ether (5 mL) at 0 °C. The reaction solution was stirred for 5 min. After separating the insoluble part, the clear ether layer was analyzed by GC-MS. ^1H NMR (500 MHz, $CDCl_3$, 298 K): δ (ppm) 7.92 (s, 1H), 7.49 (s, 1H), 3.97 (s, 3H), 1.40 (s, 9H), 1.26 (s, 9H).

Crystal Structure Analysis. Diffraction data for **5**·ClO_4 and **7**·BPh_4 were collected on a Bruker Smart APEX II (Mo Kα radiation, λ = 0.710 73 Å). Crystallographic data of the complexes are presented in Table 1. Cell refinement, indexing and scaling of the data set were carried out using the APEX2 v2.1−0 software.[48] The structures were solved by direct methods and subsequent Fourier analyses and refined by the full-matrix least-squares method based on F^2 with all observed reflections.[49] In all the complexes the hydrogen atoms were fixed. The non-hydrogen atoms were treated anisotropically.

Density Functional Theory Calculations. All intermediates and transition-state geometries were optimized in vacuum using the hybrid density functional B3LYP[50−54] along with 6-31G(d) basis functions for N, C, H, O and effective core potential LANL2 along with LANL2DZ basis set on Fe atom.[55,56] All computations were conducted using the Gaussian 09 quantum chemistry suite.[57] Gas-phase enthalpy and free-energy values were computed for 1 atmospheric pressure and 298 K temperature. Using the CPCM solvent model[58−60] for acetonitrile, relative free energy activation barriers were computed with 6-31+G(d, p) basis sets on N, C, H, O atoms; effective core potential LANL2 along with LANL2DZ on Fe atom are reported in the ensuing discussion.[56,61] For solvent phase free energy changes the solvent phase entropies of entities were used. The solvent phase entropies were derived by empirically scaling the corresponding gas phase entropies with a factor of 0.5.[62,63] This is a standard approximation that has been used in other quantum chemical studies.[64−66]

Table 1. Crystallographic Data for 5·ClO_4 and 7·BPh_4·CH_3OH

	5·ClO_4[a]	7·BPh_4·CH_3OH[b]
empirical formula	$C_{28}H_{32}ClFeN_5O_5$	$C_{60}H_{70}BFeN_5O_2$
formula weight	609.89	959.87
crystal system	monoclinic	monoclinic
space group	*P*2(1)/*n*	*P*2(1)/*c*
a, Å	17.034(7)	22.532(3)
b, Å	9.392(4)	10.964(1)
c, Å	19.457(11)	22.470(3)
α, deg	90	90.00
β, deg	114.958(10)	108.980(4)
γ, deg	90	90.00
volume, $Å^3$	2822(2)	5249.0(12)
Z	4	4
D_{calcd}, Mg/m^3	1.435	1.215
μ Mo Kα, mm^{-1}	0.676	0.335
F(000)	1272	2048
θ range, deg	1.34−22.03	0.96−26.00
reflections collected	18 825	63 203
reflns unique	3435	10 244
R(int)	0.1519	0.0486
data ($I > 2\sigma(I)$)	2260	8781
parameters refined	365	633
goodness-of-fit on F^2	1.079	1.129
R_1 [$I > 2\sigma(I)$]	0.0736	0.0526
wR_2	0.1922	0.1368

[a]Also known as [(6-Me_3-TPA)Fe^{II}(5-Me-HAP)]ClO_4. [b]Also known as [(6-Me_3-TPA)Fe^{II}(4,6-di-*t*Bu-HAP)](BPh_4)·CH_3OH.

RESULTS AND DISCUSSION

Syntheses and Characterization. Reactions of equimolar amounts of ligand and iron(II) perchlorate hydrate with respective 2-aminophenols in the presence of triethylamine under N_2 atmosphere afford the corresponding iron(II)-aminophenolate complexes (Scheme 4). The complexes are isolated either as perchlorate or tetraphenylborate salts. Although the complexes are isolated in good to moderate yields (75−41%), there is no correlation between the yield of the complex and the nature of the substituent on the aminophenolate ring. The isolated yields of the perchlorate salts are found to be low due to their high solubility in methanol. The complexes are air-stable in solid state but are extremely sensitive in solution. IR spectra of the complexes in solid state exhibit strong band at around 1600 cm^{-1} characteristic of metal-coordinated monoanionic aminophenolates.[45,67] The presence of bands due to counterions (perchlorate or tetraphenylborate) in the IR spectra suggests

dx.doi.org/10.1021/ic403043e | Inorg. Chem. 2014, 53, 4899−4912

monocationic nature of the complexes. Complex **1**·BPh_4 in acetonitrile exhibits an intense absorbance band at 378 nm in the optical spectrum, whereas other complexes show absorption band at around 400 nm (Supporting Information, Figures S1 and S2). The complexes exhibit room temperature magnetic moment values between 4.8 and 5.2 μ_B. ^{1}H NMR spectra of the complexes display paramagnetically shifted resonances of the protons in the region between −40 and 60 ppm (Supporting Information, Figures S3−S8). A comparison of ^{1}H NMR spectra of the iron(II) complexes suggests that the broad signal appeared in the upfield region between −25 ppm and −35 ppm is attributable to the resonance of α-CH_3 protons of 6-Me_3-TPA ligand.[68,69] Sharp peaks from the pyridyl protons of 6-Me_3-TPA ligand are observed in the downfield region between 35 and 50 ppm. The methylene protons are too broad to be observed in the spectra. The aromatic protons of 2-aminophenols appear in between 7 and 9 ppm. The ^{1}H NMR spectra along with the magnetic moment values strongly suggest the complexes to be mononuclear high-spin iron(II) species. Complexes **5**·ClO_4 and **7**·BPh_4 were further characterized by single-crystal X-ray diffraction. Single crystals of **5**·ClO_4 and **7**·BPh_4·CH_3OH were grown from a solvent mixture of dichloromethane, methanol and diethyl ether at room temperature.

The structure of the mononuclear complex cation of **5**·ClO_4 shows a six-coordinate iron center coordinated by four nitrogen donors from the N_4 ligand and a bidentate monoanionic aminophenolate (Figure 1). The aminophenolate ring coordinates through one phenolate oxygen (O1) and one amine nitrogen (N5) with the Fe1−O1 and Fe1−N5 distances of 1.954(5) and 2.299(7) Å, respectively (Table 2). The average Fe1−N distance of the ligand is found to be 2.250(7) Å, similar to that reported for a related complex [(6-Me_3-TPA)Fe^{II}(4-^{t}Bu-HAP)](BPh_4) (**6**·BPh_4).[45] The coordination geometry of the iron center is distorted octahedron where the axial positions are occupied by one of the pyridine nitrogens (N4) of the tetradentate ligand and the amine nitrogen (N5) of aminophenolate with the N4−Fe1−N5 angle of 171.4(2)° (Table 2). The equatorial plane is composed of O1, N1, N2, and N3 donors.

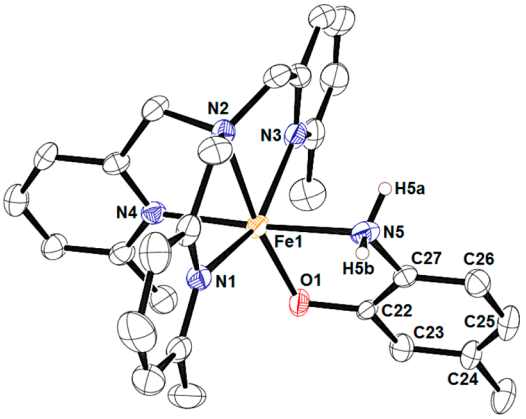

Figure 1. ORTEP plot of the complex cation of **5**·ClO_4 with 40% thermal ellipsoid parameters. The counterions and H atoms except those on N5 were omitted for clarity.

The cationic part of complex **7**·BPh_4·CH_3OH is isostructural and iso-electronic with the iron(II)-catecholate complex, [(6-Me_3-TPA)Fe^{II}(DBCH)]$^+$ (DBCH$_2$ = 3,5-di-*tert*-butylcatechol) with comparable metal−ligand bond parameters.[70] A bidentate binding motif of 2-amino-4,6-di-*tert*-butylphenolate (4,6-di-^{t}Bu-HAP) (Figure 2), similar to that in **5**·ClO_4 and **6**·BPh_4, is observed. The steric interaction between the *tert*-butyl group on the aminophenolate ring and the methyl groups on the pyridine rings of the ligand forces the metal ion to adopt a distorted octahedral coordination geometry with the axial N2−Fe1−O1 angle of 171.56(7)° (Table 2). Average C−C bond distances of 1.386 and 1.400 Å for aminophenol rings

Table 2. Selected Bond Lengths (Å) and Angles (deg) of 5·ClO_4 and 7·BPh_4·CH_3OH

bond distance/angles	**5**·ClO_4 (Å/deg)	**7**·BPh_4·CH_3OH (Å/deg)
Fe(1)−N(1)	2.317(7)	2.281(2)
Fe(1)−N(2)	2.210(7)	2.232(2)
Fe(1)−N(3)	2.264(7)	2.342(2)
Fe(1)−N(4)	2.208(7)	2.225(2)
Fe(1)−N(5)	2.299(7)	2.238(2)
Fe(1)−O(1)	1.954(5)	1.970(2)
C(22)−O(1)	1.353(9)	1.335(3)
C(27)−N(5)	1.442(10)	1.458(3)
C(22)−C(23)	1.401(11)	1.425(3)
C(23)−C(24)	1.401(12)	1.398(3)
C(24)−C(25)	1.352(13)	1.398(4)
C(25)−C(26)	1.385(13)	1.390(3)
C(26)−C(27)	1.379(12)	1.385(3)
C(27)−C(22)	1.397(12)	1.407(3)
O(1)−Fe(1)−N(1)	104.5(2)	105.60(7)
O(1)−Fe(1)−N(2)	170.5(2)	171.56(7)
O(1)−Fe(1)−N(3)	104.1(3)	105.28(7)
O(1)−Fe(1)−N(4)	109.0(2)	108.01(7)
O(1)−Fe(1)−N(5)	78.7(2)	79.99(7)
N(1)−Fe(1)−N(2)	75.9(2)	73.73(7)
N(1)−Fe(1)−N(3)	150.7(3)	148.75(7)
N(1)−Fe(1)−N(4)	84.2(2)	93.84(7)
N(1)−Fe(1)−N(5)	90.3(2)	91.90(7)
N(2)−Fe(1)−N(3)	74.8(3)	75.02(7)
N(2)−Fe(1)−N(4)	80.4(2)	80.41(7)
N(2)−Fe(1)−N(5)	91.9(2)	91.60(7)
N(3)−Fe(1)−N(4)	92.5(2)	81.08(7)
N(3)−Fe(1)−N(5)	89.1(2)	88.81(7)
N(4)−Fe(1)−N(5)	171.4(2)	168.43(7)

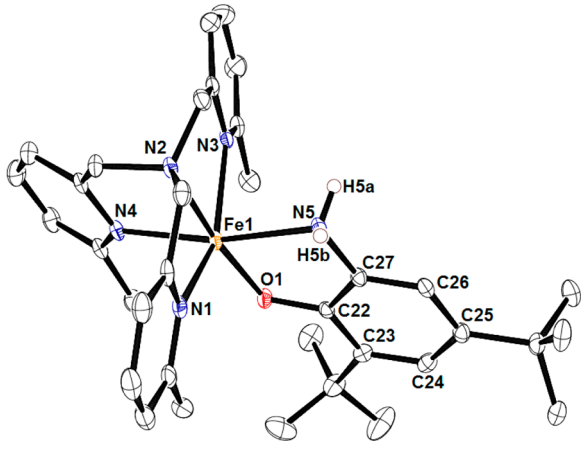

Figure 2. ORTEP plot of the complex cation of 7·BPh_4·CH_3OH with 40% thermal ellipsoid parameters. The counterions and H atoms except those on N5 were omitted for clarity.

dx.doi.org/10.1021/ic403043e | Inorg. Chem. 2014, 53, 4899−4912

in **5**·ClO_4 and **7**·BPh_4, respectively, are consistent with fully delocalized π bonding in the aromatic rings. In **5**·ClO_4, the C22−O1 and C27−N5 distances are found to be 1.353(9) and 1.442(10) Å, respectively, and for **7**·BPh_4 the distances are 1.335(3) and 1.458(3) Å, respectively (Table 2). In the complexes, the C−N bonds are typical C−N single bonds and the C−O distances are typical for organic phenolates.[36] The bond parameters are very similar to those observed in [(Tp^{Ph2})Fe^{II}(4,6-di-^{t}Bu-HAP)] and [(6-Me_3-TPA)Fe^{II}(4-^{t}Bu-HAP)](BPh_4) (**6**·BPh_4) supporting the coordination of aminophenolate to the iron center with an anionic phenolate oxygen and a neutral amine nitrogen.[43,45]

The crystal structure of the substrate bound APD reveals the binding of a suicide inhibitor, monoanionic 4-nitrocatechol, consistent with the crystal structure of homoprotocatechuate 2,3-dioxygenase.[26,35] The bidentate binding of monoanionic 2-aminophenolate to the iron(II) in biomimetic complexes[43,45] structurally mimics the enzyme−substrate adduct of 2-aminophenol dioxygenases. Although the X-ray diffraction quality single crystals could not be isolated for **1**·BPh_4, **2**·ClO_4, **3**·BPh_4, and **4**·BPh_4 after several attempts, the spectroscopic and analytical data suggest the cationic part of theses complexes to be mononuclear with six-coordinate geometry at the iron(II) center similar to that in **5**, **7**, and [(6-Me_3-TPA)Fe^{II}(4-^{t}Bu-HAP)]$^+$ (**6**).

Dioxygen Reactivity. All the iron(II)-2-aminophenolate complexes, except **1**·BPh_4, are extremely sensitive toward dioxygen in solution. Exposure of an acetonitrile solution of **2**·ClO_4 to dioxygen results in a color change from yellow to deep green. Over a period of 15 min, the charge transfer (CT) band at 402 nm disappears, and three new bands at around 365 nm, 560 and 920 nm appear (Figure 3). The new bands, in analogy

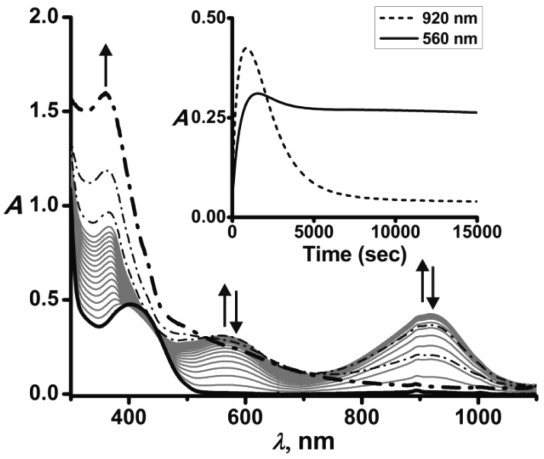

Figure 3. Time-dependent optical spectral changes during the reaction of **2**·ClO_4 with dioxygen at 298 K (concentration: 0.5 mM in acetonitrile).

to the that observed in the reaction of [(6-Me_3-TPA)Fe^{II}(4-^{t}Bu-HAP)](ClO_4) (**6**·ClO_4) with dioxygen, are assigned to the 2-amidophenolate-to-iron(III) charge-transfer.[45,67] The solution exhibits a molecular ion peak at m/z = 494.03 with the isotope distribution pattern calculated for [(6-Me_3-TPA)Fe(AP)]$^+$. The spectral data of the reaction solution after 15 min thus support the formation of an iron(III)-2-amidophenolate species, [(6-Me_3-TPA)Fe^{III}(AP)](ClO_4). Further exposure of the green solution to dioxygen slowly yields an orange solution during which time the 920 nm band diminishes with concomitant formation of a relatively sharp band at 360 nm. The EPR signal changes as the reaction progresses and the final oxidized solution exhibits a rhombic EPR signals at g = 4.2 along with a signal at g = 1.99 (Supporting Information, Figure S9).

The ^{1}H NMR spectrum of the organic product derived from 2-aminophenol after acidic work-up of the final oxidized solution of **2**·ClO_4 shows proton resonances in between 6 and 8 ppm attributable to aromatic protons (Supporting Information, Figure S10). The positions of the proton resonances match well with those of 2-amino-3*H*-phenoxazin-3-one.[71] In the reaction, about 85% 2-amino-3*H*-phenoxazin-3-one was quantified by ^{1}H NMR spectroscopy. The weak signals in the ^{1}H NMR spectrum may arise from other auto-oxidation products from 2-aminophenol. EPR and optical spectral data of the final reaction solution suggest the presence of a mixture of iron(III) species and 2-aminophenolate derived products. The C−C bond cleavage product (2-picolinic acid) is not observed in the reaction (Supporting Information, Figure S10b). The reaction of an equimolar mixture of iron(II) perchlorate hydrate and 2-aminophenol affords the same auto-oxidation product (Supporting Information, Figure S10c). It can therefore be concluded that the reaction of **2**·ClO_4 with dioxygen forms 2-amino-3*H*-phenoxazin-3-one via an auto-oxidation pathway (Scheme 5). The formation of 2-amino-3*H*-phenoxazin-3-one from 2-aminophenol on iron(II) complex is reminiscent of the reactions catalyzed by 2-aminophenol oxidase and tyrosinase.[72]

Scheme 5. Reaction of [(6-Me_3-TPA)Fe^{II}(HAP)]$^+$ (2) with Dioxygen

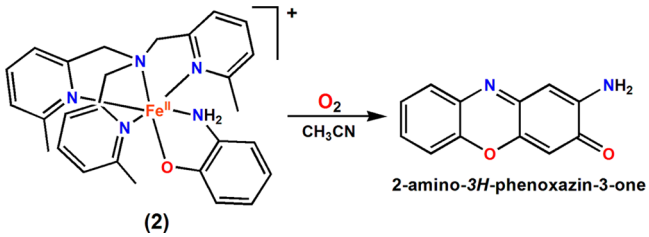

The reactions of complexes **3**·BPh_4, **4**·BPh_4, and **5**·ClO_4 with dioxygen, on the contrary, involve three consecutive steps. In the first step, the yellow solutions of the complexes turn dark green immediately upon exposure to dioxygen. For [(6-Me_3-TPA)Fe^{II}(3-Me-HAP)](BPh_4) (**3**·BPh_4), the charge transfer band at around 401 nm disappears with the formation of two intense bands at around 620 and 935 nm within 5 min (Figure 4a). X-band EPR spectrum of the green solution exhibits a signal at g = 4.2 supports the formation of a rhombic iron(III) species in the first step (Supporting Information, Figure S11). A molecular ion peak at m/z = 509.21 with the isotope distribution pattern calculated for [(6-Me_3-TPA)Fe(3-Me-AP]$^+$ is observed in the ESI-mass spectrum of the green solution (Figure 5a). The first step thus involves the generation of an iron(III)-2-amidophenolate species.

Further exposure of the dark green solution to dioxygen leads to a faint green solution. During the time period of 12 min, the sharp band at 935 nm disappears with concomitant formation of a distinct absorption band at 645 nm (Figure 4b). During the reaction a signal is appeared at g = 8.4 in the EPR spectrum (Supporting Information, Figure S11). The band at 645 nm then slowly decays to form a light orange solution over a period of 16 h (Figure 4c). The final reaction solution

dx.doi.org/10.1021/ic403043e | Inorg. Chem. 2014, 53, 4899−4912

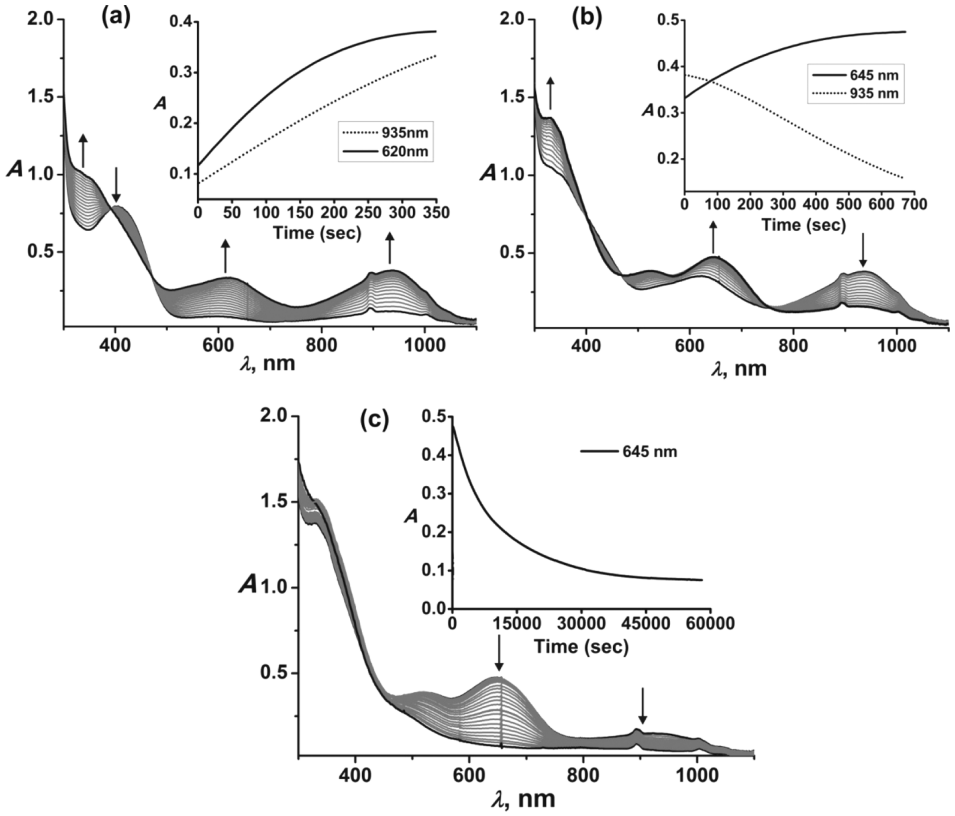

Figure 4. Optical spectral changes with time during the reaction of **3**·BPh_4 (0.5 mM in acetonitrile) with dioxygen at 298 K for (a) initial 5 min, (b) for the next 12 min, and (c) for the next 16 h.

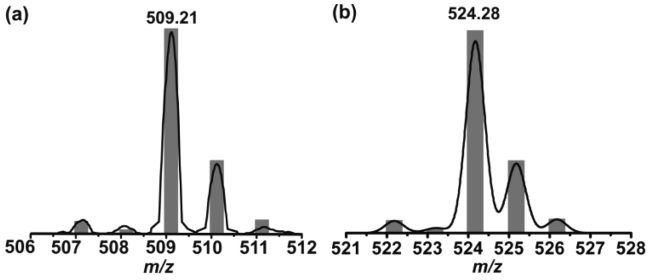

Figure 5. ESI-mass spectra of the species formed (a) after 5 min and (b) at the end of the reaction of **3**·BPh_4 with dioxygen at 298 K. The bar plots represent the simulated isotopic distribution pattern for (a) $[(6\text{-}Me_3\text{-TPA})Fe(3\text{-Me-AP})]^+$ and (b) $[(6\text{-}Me_3\text{-TPA})Fe(3\text{-Me-2-picolinate})]^+$.

displays a rhombic signal at $g = 4.2$ along with a weak signal at $g = 1.99$ in the EPR spectrum (Supporting Information, Figure S11). Similar changes in the optical and EPR spectra are observed for complexes **4**·BPh_4 and **5**·ClO_4 (Supporting Information, Figures S12, S13a, S14a, S13b, and S14b) The ESI−mass spectrum of the final oxidized solution of **3**·BPh_4 show ion peak at $m/z = 524.28$ with the isotope distribution calculated for $[(6\text{-}Me_3\text{-TPA})Fe(3\text{-Me-2-picolinate})]^+$ (Figure 5b). Final oxidized solutions of **4**·BPh_4 and **5**·ClO_4 also display similar ESI-mass spectra.

^{1}H NMR spectra of organic products obtained from the final oxidized solutions of the iron(II) complexes of methyl substituted aminophenolates display three proton resonances in the aromatic region between 7.5 and 8.6 ppm along with one sharp singlet at around 2.25 ppm (see Experimental Section). Although the peaks from organic products in all three cases appear almost at the same positions, the multiplicity and the peak area of the proton resonances strongly support the formation of 5-methyl-2-picolinic acid from **5**·ClO_4 (Figure 6), 3-methyl-2-picolinic acid from **3**·BPh_4 and 4-methyl-2-picolinic acid from **4**·BPh_4 (Supporting Information, Figure S15 and Scheme 6). In all the cases, no unreacted aminophenol is observed at the end of the reaction. The methyl substituted

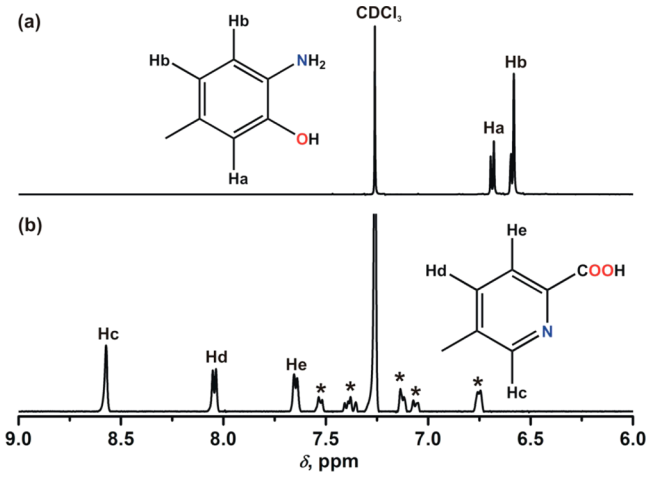

Figure 6. ^{1}H NMR spectra (500 MHz, 295 K, $CDCl_3$) of (a) 2-amino-5-methylphenol and (b) the organic product obtained from the oxidized solution of **5**·ClO_4. The peaks marked as * represent the fragments from the 6-Me_3-TPA ligand, and the peak marked as # is the residual $CHCl_3$ in $CDCl_3$.

dx.doi.org/10.1021/ic403043e | Inorg. Chem. 2014, 53, 4899−4912

Scheme 6. Reaction of the Iron(II)-2-aminophenolate Complexes with Dioxygen and the C−C Cleavage Products

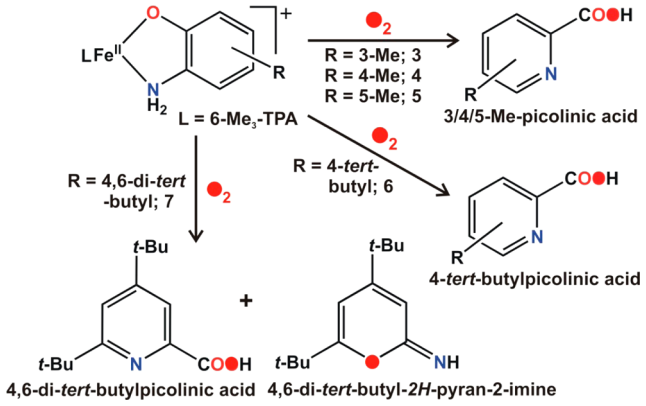

aminophenolates are quantitatively converted to the corresponding 2-picolinic acids.

On the contrary, the spectral change during the reaction of 7·BPh_4 with oxygen is completely different than that observed with other complexes discussed above. In the reaction, the CT band at 402 nm decays and two new bands at 520 and 665 nm are formed over a period of 10 min in acetonitrile at 298 K (Figure 7a). The ESI-mass spectrum of the solution exhibits a molecular ion peak at m/z = 565.23 with the isotopic distribution calculated for $[(6\text{-}Me_3\text{-TPA})Fe(4,6\text{-di-}^t\text{Bu-AP})]^+$. The green solution displays a rhombic EPR signal at g = 4.2 typical of a high-spin iron(III) species. Additionally a sharp signal at g = 1.99 is observed possibly due to the presence of a ligand-based radical species in solution (Figure 8). The intensity of the EPR signal at g = 1.99 slowly diminishes as the reaction proceeds. After 10 min, the CT bands at 520 and 665 nm slowly decay over a period of 22 h (Figure 7b). Although the final oxidized complex could not be analyzed by ESI-MS, the X-band EPR spectrum suggests the formation of a high-spin iron(III) species (Figure 8).

The organic products from the oxidized solution of 7·ClO_4 were isolated by acidic work-up and subsequent extraction with diethyl ether for analysis by ^{1}H NMR and GC-MS. The ^{1}H NMR spectrum of organic products shows three sharp singlets at 8.07, 7.59, and 6.05 ppm (Figure 9). The sharp signals observed in the range of 1.44−1.16 ppm represent the aliphatic protons of the *tert*-butyl groups. The absence of aromatic protons at 6.81 and 6.91 ppm strongly suggests that no

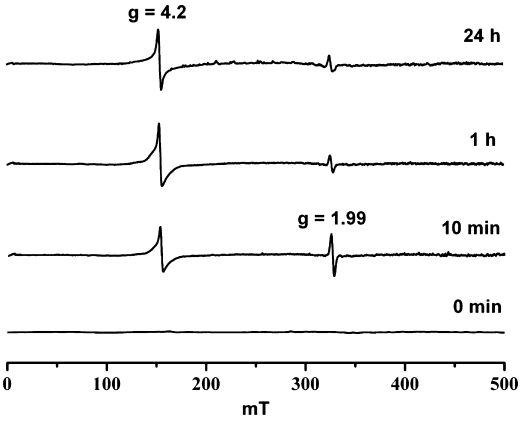

Figure 8. X-band EPR spectral changes with time during the reaction of 7·BPh_4 with dioxygen in acetonitrile. (Experimental conditions: temperature = 77 K, microwave frequency = 9.10 GHz, microwave power = 0.998 mW, modulation amplitude = 100 kHz, modulation width = 1 mT, time constant = 0.03 s).

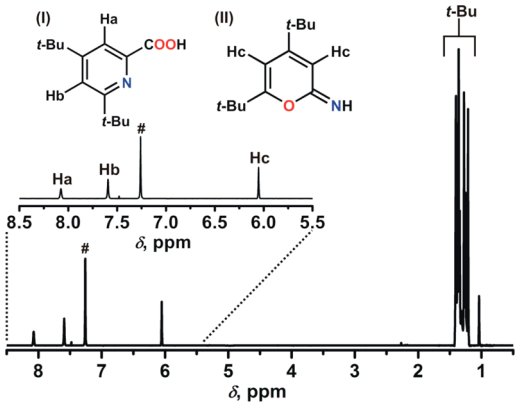

Figure 9. ^{1}H NMR spectrum (500 MHz, 295 K, $CDCl_3$) of the organic products obtained from the final oxidized solution of 7·ClO_4 after removal of the metal ion. The peak marked as # is the residual $CHCl_3$ in $CDCl_3$.

unreacted 4,6-di-^{t}Bu-HAP is present in the oxidized solution. The protons of 4,6-di-*tert*-butyl-2*H*-pyran-2-one, an extradiol cleavage product from 3,5-di-*tert*-butylcatechol, exhibit a singlet resonance at 6.05 ppm in the ^{1}H NMR spectrum. These results unambiguously support the formation of 4,6-di-*tert*-butyl-2*H*-pyran-2-imine via oxidative C−C cleavage of 4,6-di-^{t}Bu-HAP.

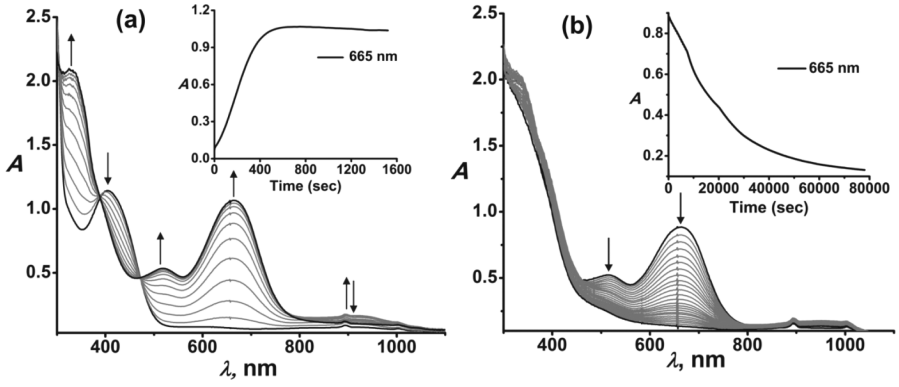

Figure 7. Optical spectral changes during the reaction of 7·BPh_4 (0.5 mM solution in acetonitrile) with dioxygen at 298 K (a) over a time period of 10 min and (b) over the next 22 h.

dx.doi.org/10.1021/ic403043e | *Inorg. Chem.* 2014, 53, 4899−4912

Comparing the ^{1}H NMR spectrum of 4-*tert*-butylpicolinic acid derived from 4-^{t}Bu-HAP,[45] the sharp singlets at 8.07 and 7.59 ppm are assigned to the aromatic protons of 4,6-di-*tert*-butylpicolinic acid (Scheme 6). The organic products, 4,6-di-*tert*-butyl-2*H*-pyran-2-imine (35%) and 4,6-di-*tert*-butyl-2-picolinic acid (65%), are quantified by calculating the relative ratio of the aromatic protons. For further confirmation, the organic products obtained from the oxidized solution of 7·ClO_4 were treated with a freshly prepared diazomethane solution. In addition to sharp peaks between 1.12 and 1.51 ppm, four singlet resonances at 7.92, 7.49, 6.05, and 4.00 ppm are observed in the ^{1}H NMR spectrum confirming the formation of methyl-4,6-di-*tert*-butyl-2-picolinate and 4,6-di-*tert*-butyl-2*H*-pyran-2-imine in the reaction (Supporting Information, Figure S16). GC-MS analysis of the organic products after esterification shows two distinct ion peaks at m/z = 208 and 249 with the expected fragmentation patterns of 4,6-di-*tert*-butyl-2*H*-pyran-2-one and methyl-4,6-di-*tert*-butyl-2-picolinate (Figure 10a,b). The imine product gets hydrolyzed during

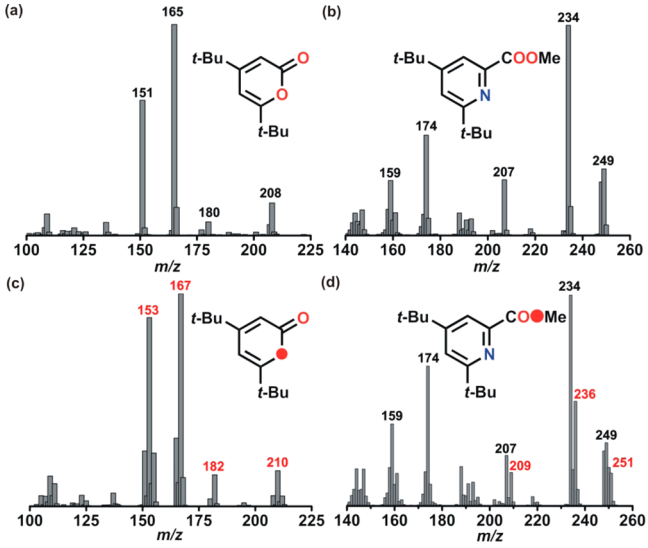

Figure 10. GC-mass spectra of organic products obtained after removal of metal ion and subsequent treatment of a freshly prepared diazomethane after reaction of 7·ClO_4 with $^{16}O_2$ (a, b) and with $^{18}O_2$ (c, d).

acidic work-up to form 4,6-di-*tert*-butyl-2*H*-pyran-2-one. The ESI-mass spectrum also supports the formation of these two products (Supporting Information, Figure S17). It is important to mention here that the iron(II)-catecholate complex, [(6-Me$_3$-TPA)Fe^{II}(DBCH)]$^+$, of the same ligand yields only intradiol cleavage products, 3,5-di-*tert*-butyl-1-oxacyclohepta-3,5-diene-2,7-dione (53%) and 3,5-di-*tert*-butyl-5-(carboxymethyl)-2-furanone (36%).[70]

The reaction of 7·ClO_4 with $^{18}O_2$ was carried out to establish the source of oxygen atoms into the cleavage products. The organic phase was treated with diazomethane and was analyzed by GC-MS. The ion peaks are shifted two mass unit higher for 4,6-di-*tert*-butyl-2*H*-pyran-2-one and methyl-4,6-di-*tert*-butyl-2-picolinate. The isotope distribution patterns for 4,6-di-*tert*-butyl-2*H*-pyran-2-one and methyl-4,6-di-*tert*-butyl-2-picolinate observed in the spectra (Figure 10c,d) support the incorporation of one ^{18}O atom into each product. While 80% incorporation of labeled oxygen into pyrone is observed, only 40% incorporation of one oxygen atom into picolinate takes place. The ESI-mass spectrum also supports the incorporation of one oxygen atom into each organic product derived from 4,6-di-^{t}Bu-HAP (Supporting Information, Figure S18). Mixed labeling experiment with $^{16}O_2$ and $H_2{}^{18}O$ shows the incorporation of one oxygen atom from water into picolinic acid (Supporting Information, Figure S19).

To understand the pathway for the reaction of 7·BPh_4 with oxygen, controlled one-electron chemical oxidation of 7·BPh_4 using a stoichiometric amount of $KMnO_4$ was carried out under nitrogen environment to isolate 7^{Ox}·BPh_4. Unfortunately, all attempts to isolate single crystals of 7^{Ox}·BPh_4 failed. The acetonitrile solution of 7^{Ox}·BPh_4 is dark green in color and exhibits sharp bands at 366 nm (ε = 3000 cm^{-1} M^{-1}), 618 nm (ε = 1900 cm^{-1} M^{-1}) and 925 nm (ε = 2700 cm^{-1} M^{-1}) under nitrogen environment (Figure 11). Three prominent signals at

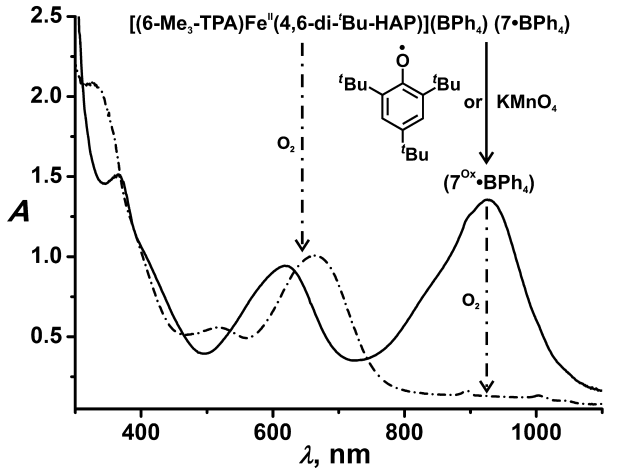

Figure 11. Optical spectra of 7^{Ox}·BPh_4 (0.5 mM in acetonitrile) under nitrogen atmosphere (bold line) and after exposure to dioxygen (dash dot line).

around g = 8.6, 5.07, and 3.71 are observed in the EPR spectrum at 77K describing an S = 5/2 spin system in solution (Supporting Information, Figure S20). Therefore, the controlled chemical oxidation of 7·BPh_4 leads to the formation of an iron(III) species [(6-Me$_3$-TPA)Fe^{III}(4,6-di-^{t}Bu-AP)](BPh_4) (7^{Ox}·BPh_4). An instantaneous decay of the band at 925 nm followed by a concomitant shift of the band at 618 to 665 nm is observed upon exposure of an acetonitrile solution of 7^{Ox}·BPh_4 to dioxygen (Figure 11).

Complex **6**·ClO_4 has been reported to react with dioxygen over a period of 6 h yielding 4-*tert*-butyl-2-picolinic acid as the only product (Scheme 6). Labeling experiment with $^{18}O_2$ supports the incorporation of one ^{18}O atom into 4-*tert*-butyl-2-picolinic acid. Additionally, a mixed labeling experiment with $^{16}O_2$ and $H_2{}^{18}O$ exhibits about 30% incorporation of one oxygen atom from water into picolinic acid.[45] At room temperature, **6**·ClO_4 reacts with dioxygen to form a species which exhibits three bands at 366 nm, 600 and 934 nm. The corresponding iron(III) species (**6**^{Ox}) prepared by oxidation with $KMnO_4$ shows similar spectral features.[45] On the contrary, when the reaction of an acetonitrile solution of **6**·ClO_4 with dioxygen is carried out at 248 K (Figure 12), the optical spectral changes closely match with those observed in the reaction of 7·BPh_4 with O_2 at room temperature. The X-band EPR spectrum of the species obtained from **6**·ClO_4 at 248 K

dx.doi.org/10.1021/ic403043e | Inorg. Chem. 2014, 53, 4899−4912

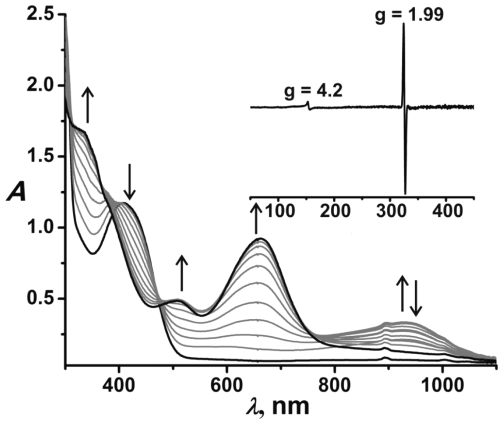

Figure 12. Change in optical spectra during the reaction of **6**·ClO_4 (0.5 mM in acetonitrile) with dioxygen at 248 K. (inset) X-band EPR spectrum of the green species at 77 K.

shows a weak rhombic signal at g = 4.2 and an isotropic signal at g = 1.99 (Figure 12).

In the oxidative C−C bond cleavage pathway, the iron complexes of alkyl substituted aminophenolates form intermediate species that display broad absorption features between 450 and 700 nm. Similar spectral features have been reported for M-iminobenzosemiquinonate (M-ISQ) complexes (M = Co(III), Ni(II), Cu(II), Fe(II), and Fe(III))[37,41,43,44,67,73] and for a structurally characterized 4,6-di-*tert*-butyl-2-*tert*-butyliminosemiquinone species.[74] In analogy to the spectra reported for M-ISQ complexes, the absorption features may be attributed to the intraligand transitions of ISQ radical. Therefore, formation of iron(II)-2-iminobenzosemiquinonate intermediate ([(L)-Fe^{II}(ISQ)]$^+$) is proposed in the reaction of iron-aminophenolate complexes with dioxygen. The EPR spectra exhibiting isotropic signal at g = 1.99 support the formation of ISQ radical species. For **7**·BPh_4, the [(L)Fe^{II}(ISQ)]$^+$ species is formed directly from the iron(II)-aminophenolate complex via ligand-centered oxidation. Two *tert*-butyl groups on the aminophenolate ring in **7**·BPh_4 stabilize the resulting ISQ radical to be observed at room temperature. Whereas, in complex **6**·ClO_4, one *tert*-butyl group present on the aminophenolate ring cannot stabilize the corresponding ISQ radical to be observed at 298 K, but the formation of the iron(II)-ISQ species is observed at low temperature. In both the cases, however, a small amount of iron(III)-amidophenolate species is also formed initially which subsequently converts to the radical intermediate.

For all other cases, [(L)Fe^{II}(ISQ)]$^+$ species is formed in the reaction of [(L)Fe^{II}(HAP)]$^+$ with dioxygen via [(L)Fe^{III}(AP)]$^+$ species. Generation of a species with absorption bands at 520 and 665 nm upon exposure of the iron(III)-imidophenolate complex **7**^{Ox}·BPh_4 to dioxygen supports this proposal. Dioxygen is probably involved in controlling the formation of radical intermediate from [(L)Fe^{III}(AP)]$^+$ species. It is conjectured that [(L)Fe^{III}(AP)]$^+$ reacts with dioxygen to form iron(III)-iminobenzosemiquinonate species ([(L)-Fe^{III}(ISQ)]$^{2+}$) and superoxide radical anion (Scheme 7). The resulting superoxide radical anion again participates in the reduction of [(L)Fe^{III}(ISQ)]$^{2+}$ to generate [(L)Fe^{II}(ISQ)]$^+$ species via outer-sphere mechanism.[75] The radical intermediate further activates dioxygen to exhibit the C−C bond cleavage reactivity.

Scheme 7. Proposed Mechanism for the Formation of Iron(II)-2-iminobenzosemiquinonate Species

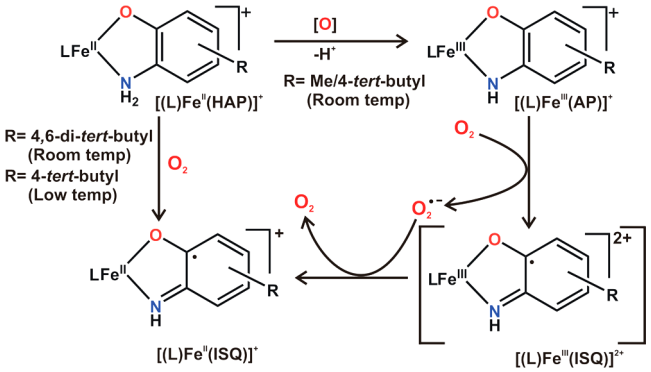

Density Functinal Theory Calculations. DFT calculations were conducted on [(6-Me_3-TPA)Fe^{III}(4-^{t}Bu-HAP)]$^+$ (**6**^{Ox}) to unravel the probable reaction pathways of regioselective C−C bond cleavage of 2-aminophenols. As observed experimentally, an iron(II)-2-aminophenolate complex (**A**) reacts rapidly with dioxygen to form an iron(III)-2-amidophenolate (**B**) via an outer sphere one-electron oxidation process. The plausible pathway for the formation of iron(III)-peroxo species from a six-coordinate iron(III)-2-amidophenolate (**B**) was investigated (Figure 13). The free-energy difference between the sextet and

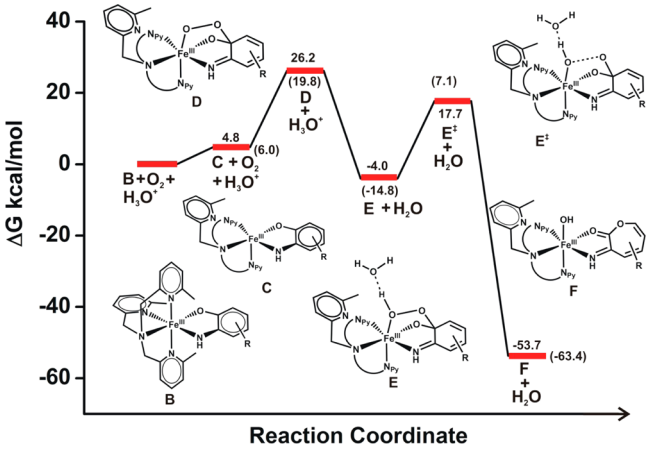

Figure 13. Free-energy profile of the reaction of **6**^{Ox} with dioxygen on quartet surface. Corresponding relative ΔH values are provided in the parentheses.

quartet spin state of **B** is predicted to be 11.1 kcal/mol, where the former is more stable with Fe−N_{amide} and Fe−$O_{phenolate}$ distances of 2.156 and 1.991 Å, respectively. In fact the ground electronic state of **B** is the sextet electronic state. However, **B** being a six-coordinate iron center, dioxygen activation at the metal center is not favored. In analogy to the mechanism proposed for the oxidative decarboxylation of a six-coordinate iron(II)-α-hydroxy acid complex [(6-Me_3-TPA)-Fe^{II}(mandelate)](BPh_4) reported by Paine et al., it can be suggested that the dissociation of one of the pyridyl arms from the metal center results in a five-coordinate iron(III)-2-phenolate (**C**) species providing a vacant site on the metal for dioxygen activation to form an iron(III)-peroxo species (**D**).[69] Dissociation of the iron imide bond could also be another possibility for the formation of the iron(III)-peroxo species. Optimization of the iron(III)-peroxo species was

dx.doi.org/10.1021/ic403043e | Inorg. Chem. 2014, 53, 4899−4912

performed considering both the possibilities. However, calculations suggest that there exists a stable intermediate after dissociation of one pyridyl arm in sextet spin state of the metal complex, but no minima could be located for iron-imide bond dissociation. This result strongly indicates that the initial oxygen activation by **B** involves opening of a pyridyl arm from the metal center. The ground electronic state of **C**, a five-coordinate complex formed by the dissociation of the pyridyl ligand arm is predicted to be the sextet spin state. **C** is 4.8 kcal/mol higher in free energy compared to **B** for the sextet spin state of the metal complex. Of note, the dissociation of a pyridyl arm for the iron(II) complex is predicted to be more endothermic and the separation between the six-coordinate iron(II) complex and the five-coordinate iron(II) complex is estimated to be 7.98 kcal/mol (Supporting Information, Figure S21). The reaction of **C** with dioxygen proceeds on a quartet surface that results from electron pairing of the triplet dioxygen which has two unpaired electrons interacting with two opposite spin electrons out of the five unpaired electrons of the sextet spin metal complex (Supporting Information, Figure S22). As reported earlier by Georgiev and co-workers the peroxo species is formed on a quartet surface.[76] The highest occupied singly occupied molecular orbital (SOMO), which has significant contributions from orbitals of the aminophenolate ligand in the metal complex, indicates that dioxygen is activated by $([(L)Fe^{II}(ISQ)]^{+}$ (**C′**). So in this case, dioxygen is activated by both the substrate and the metal center. The substantial mixing of the metal-substrate orbitals in the SOMO precludes the formation of a metal ligated superoxo species in these calculations. The resulting quartet iron(III)-peroxo species (**D**) lies 26.2 kcal/mol above with respect to the reactants. In the optimized geometry of the peroxo species (**D**) the Fe−O, O−O, and C−O distances are found to be 1.796, 1.448, and 1.448 Å, respectively (Supporting Information, Figure S23). The homolytic cleavage of O−O bond of the peroxo species (**D**) on the quartet surface was studied. The free-energy activation barrier involved in this process is a staggering 41.9 kcal/mol. A large O−O dissociation energy on the quartet state indicates that the C−C bond cleavage does not take place via homolytic O−O bond dissociation route.

It was suggested earlier that the loss of a proton occurs during the formation of iron(III)-2-amidophenolate (**B**) from the corresponding iron(II)-2-aminophenolate complex. This proton plays a crucial role in the O−O bond cleavage step. A protonated peroxo species may form in the reaction pathway as a reactive intermediate. The role of proton in the regioselective C−C bond cleavage of catechol has recently been implicated.[77] The solvent acetonitrile is not a good proton acceptor. However, like any other solvents it is likely to contain trace amounts of water. The highly polar water molecules are expected to cluster around the charged ionic species in acetonitrile medium. Water molecules can accept protons and release those protons to facilitate reactions. To mimic such a condition a H_3O^{+} was included in the computational model, which takes into account the lost proton in the first oxidation step of conversion of **A** to **B**. It was found that a hyrdronium can act as a proton source and can protonate one of the peroxo oxygens favorably in **E**. Optimized structure of **E** on the quartet surface shows that the hydroperoxide group ligated to the iron(III) center is positioned axially with respect to the amidophenolate ring (Figure 14). In such geometry, the O−O bond is aligned antiperiplanar with the C1−C6 bond, which is an essential requirement for obtaining selective cleavage

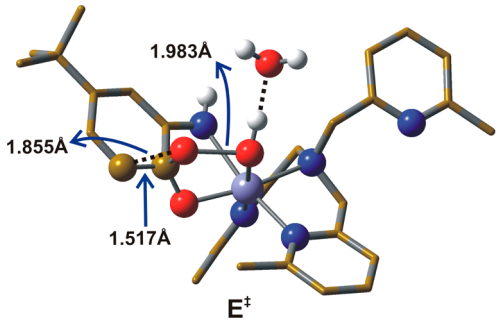

Figure 14. Transition-state geometry of the protonated peroxo species in quartet state.

product.[20] The heterolytic O−O bond dissociation free-energy barrier of the protonated peroxo species (**E**) to form C−C cleaved product (**F**) was calculated. The required free-energy activation barrier for O−O bond cleavage is 21.7 kcal/mol on the quartet surface, which indicates that the reaction pathway is feasible under the aforementioned experimental conditions. Formation of the C−C cleavage product, a seven member lactone ring, is highly exoergic (calculated 53.7 kcal/mol) in nature. Computational studies reveal that one of the pyridine rings *cis* to the aminophenolate ring gets dissociated from the coordination site for dioxygen activation and a proton is essential to trigger the heterolytic O−O bond cleavage. The antiperiplanar arrangement of C1−C6 bond with the O−O bond of protonated-peroxide results in selective C−C bond cleavage product.

The presence of an electron withdrawing nitro group at the 4-position on the aminophenolate ring in **1** makes it unreactive toward dioxygen. Two-electron oxidation of 2-aminophenol to iminoquinone followed by coupling with another molecule of 2-aminophenol is observed in the reaction of 2 resulting in phenoxazinone product. However, incorporation of electron donating groups such as methyl (3-Me-HAP; **3**/4-Me-HAP; **4**/5-Me-HAP; **5**), *tert*-butyl (4-^{t}Bu-HAP; **6** and 4,6-di-^{t}Bu-HAP; **7**) results in oxygenolytic aromatic ring cleavage reaction (Scheme 6). It is expected that other electron-withdrawing group such as CN would make the iron(II) complex inert toward dioxygen. A more strongly electron donating substituent such as OMe is expected to show faster C−C bond cleavage reactivity. The substitutions on the aminophenolate ring control the stability of the O_2-activating iron(II)-2-iminobenzosemiquinonate species. The intermediate gets stabilized by two *tert*-butyl groups on the aminophenolate ring and as a result complex **7** exhibits slow reactivity compared to complex **6** (22 h for **7** vs 6 h for **6**). Total time required for the reaction of iron(II) complexes of methyl substituted aminophenolates depends on the position of methyl group on the aromatic ring. While complex **4** requires about 1 h 50 min, complexes **3** and **5** take about 16.5 and 8.5 h, respectively.

Although the iron(II)-2-iminobenzosemiquinonate species could not be isolated, a mechanism is proposed on the basis of experimental results and theoretical calculations (Scheme 8). The iron(II)-2-aminophenolate complex (**A**) initially reacts with oxygen to form an iron(III)-2-amidophenolate (**B**) species as depicted for the reported iron(II)-catecholate and iron(II)-aminophenol complexes.[47,67,70] Dissociation of one of the pyridyl arms from the metal center of **B** results in a five-coordinate iron(III)-2-amidophenolate (**C**). The redox isomer of **C**, an iron(II)-2-iminobenzosemiquinonate species (**C′**) then

dx.doi.org/10.1021/ic403043e | *Inorg. Chem.* 2014, 53, 4899−4912

Scheme 8. Proposed Mechanism for the Aromatic C−C Bond Cleavage of 2-Aminophenols on Biomimetic Iron Complex

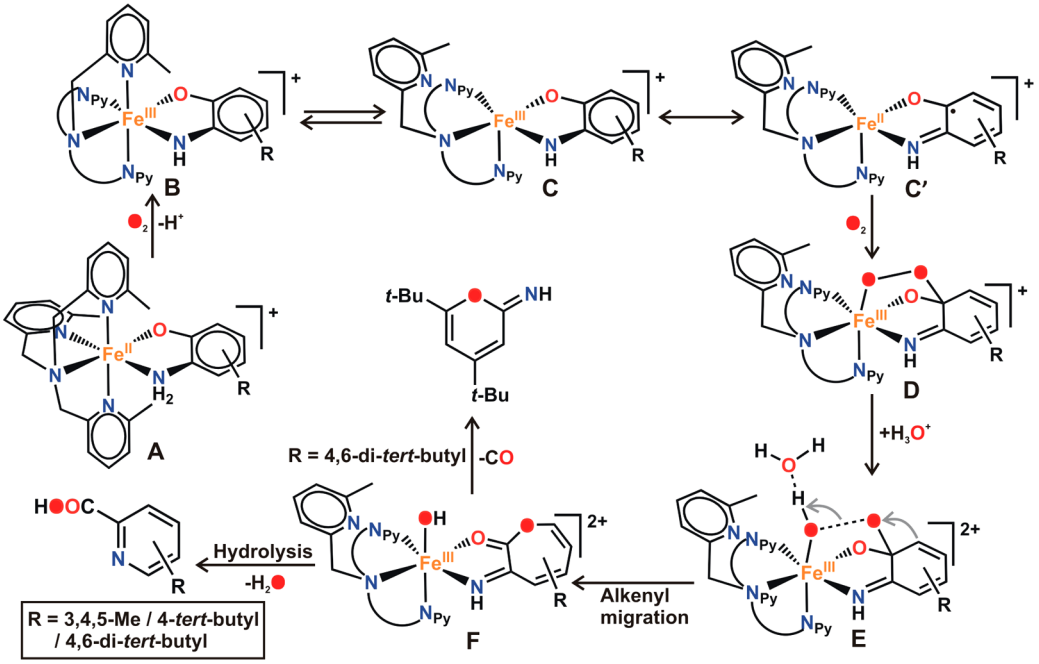

reacts further with oxygen to form iron(III)-peroxide (**D**). Theoretical studies with the extradiol catechol dioxygenases suggest that initially oxygen activation occurs at the metal center followed by an attack of iron(III)-superoxide to the substrate to form a peroxo intermediate.[78] The protonation of iron(III)-peroxide (**D**) species preferably at the oxygen attached to the metal center results in a protonated peroxo species **E**. Heterolytic O−O bond cleavage of the protonated peroxo species (**E**) through alkenyl migration leads to the formation of a lactone intermediate (**F**). Muconic acid semialdehyde is formed via hydrolysis of the lactone species by the metal-coordinated hydroxide. A subsequent rearrangement followed by loss of a water molecule forms picolinic acid. Loss of a CO molecule from the lactone yields pyranimine product observed for **7**.

CONCLUSION

We isolated and characterized a series of iron(II)-2-aminophenolate complexes supported by a tripodal N_4 ligand. The diverse substitution on aminophenolate ring offers different electronic environment of the corresponding iron(II) complexes. X-ray crystal structures reveal six-coordinate iron(II) center in the cationic complexes with bidentate binding of the monoanionic aminophenolates. The iron(II)-4-nitroaminophenolate complex is unreactive toward dioxygen which bears resemblance to 4-nitrocatechol, the suicide inhibitor of 2-aminophenol dioxygenases and catechol dioxygenases. The iron(II)-2-aminophenolate complex reacts with dioxygen to form 2-amino-3*H*-phenoxazin-3-one and the reactivity pattern is similar to that of aminophenol oxidase or tyrosinase. The C−C cleavage product, 2-picolinic acid is observed in the reaction of alkyl substituted aminophenolate complexes with molecular oxygen. On the other hand, the reaction of iron(II)-2-amino-4,6-di-*tert*-butylphenolate complex with oxygen results in a mixture of 4,6-di-*tert*-butyl-2*H*-pyran-2-imine and 4,6-di-*tert*-butyl-2-picolinic acid. The products are found to be regioselective and are resulted from the C1−C6 bond cleavage of the coordinated 2-aminophenolates. $^{18}O_2$ labeling experiments clearly demonstrate the incorporation of one oxygen atom from molecular oxygen into the cleavage products. The oxidative transformation of substituted 2-aminophenols to the corresponding picolinic acids on an iron(II) complex in a single step using molecular oxygen functionally mimic the activity of 2-aminophenol dioxygenases. Experimental results and DFT calculations indicate the involvement of an iron(II)-2-iminobenzosemiquinonate species in the reaction pathway. The results described herein show the influence of substituent on the C−C bond cleavage of aminophenols. This mechanistic information would provide useful insight into the development of catalytic functional models of 2-aminophenol dioxygenases.

ASSOCIATED CONTENT

Supporting Information

Crystallographic data in CIF format, electronic spectra, ESI-mass spectra, GC-mass spectra, EPR spectra, NMR spectra, and DFT-optimized geometries. This material is available free of charge via the Internet at http://pubs.acs.org.

AUTHOR INFORMATION

Corresponding Author

*E-mail: ictkp@iacs.res.in. Fax: +91-33-2473-2805. Phone: +91-33-2473-4971.

Notes

The authors declare no competing financial interest.

ACKNOWLEDGMENTS

We gratefully acknowledge the Department of Science and Technology (DST), Government of India (Project SR/S1/IC-51/2010), and the Indian National Science Academy (Project for INSA Young Scientist Awardee) for financial support. X-ray diffraction data were collected at the DST-funded National Single Crystal Diffractometer Facility at the Department of Inorganic Chemistry, Indian Association for the Cultivation of

Science. B.C. and S.B. acknowledge the Council of Scientific and Industrial Research (CSIR), India, for research fellowships.

DEDICATION

[§]Dedicated to Professor Phalguni Chaudhuri on the occasion of his 70th birthday.

REFERENCES

(1) Fetzner, S.; Tshisuaka, B.; Lingens, F.; Kappl, R.; Hüttermann, J. *Angew. Chem., Int. Ed.* **1998**, *37*, 576.
(2) Fetzner, S. *Appl. Environ. Microbiol.* **2012**, *78*, 2505.
(3) Fuchs, G.; Boll, M.; Heider, J. *Nat. Rev. Microbiol.* **2011**, *9*, 803.
(4) Gibson, D. T.; Parales, R. E. *Curr. Opin. Biotechnol.* **2000**, *11*, 236.
(5) Vaillancourt, F. H.; Bolin, J. T.; Eltis, L. D. *Crit. Rev. Biochem. Mol. Biol.* **2006**, *41*, 241.
(6) Ferraroni, M.; Matera, I.; Bürger, S.; Reichert, S.; Steimer, L.; Scozzafava, A.; Stolz, A.; Briganti, F. *FEBS J.* **2013**, *280*, 1643.
(7) Hintner, J.-P.; Lechner, C.; Riegert, U.; Kuhm, A. E.; Storm, T.; Reemtsma, T.; Stolz, A. *J. Bacteriol.* **2001**, *183*, 6936.
(8) Lipscomb, J. D.; Orville, A. M. In *Metal Ions in Biological Systems;* Sigel, H., Sigel, A., Eds.; Marcel Dekker: New York, 1992; Vol. *28*, p 243.
(9) Costas, M.; Mehn, M. P.; Jensen, M. P.; Que, L., Jr. *Chem. Rev.* **2004**, *104*, 939.
(10) Kovaleva, E. G.; Neibergall, M. B.; Chakrabarty, S.; Lipscomb, J. D. *Acc. Chem. Res.* **2007**, *40*, 475.
(11) Lendenmann, U.; Spain, J. C. *J. Bacteriol.* **1996**, *178*, 6227.
(12) Harpel, M. R.; Lipscomb, J. D. *J. Biol. Chem.* **1990**, *265*, 22187.
(13) Titus, G. P.; Mueller, H. A.; Burgner, J.; Rodríguez de Córdoba, S.; Peñalva, M. A.; Timm, D. E. *Nat. Struct. Biol.* **2000**, *7*, 542.
(14) Machonkin, T. E.; Doerner, A. E. *Biochemistry* **2011**, *50*, 8899.
(15) Xu, L.; Resing, K.; Lawson, S. L.; Babbitt, P. C.; Copley, S. D. *Biochemistry* **1999**, *38*, 7659.
(16) Hintner, J.-P.; Reemtsma, T.; Stolz, A. *J. Biol. Chem.* **2004**, *279*, 37250.
(17) Ju, K.-S.; Parales, R. E. *Microbiol. Mol. Biol. Rev.* **2010**, *74*, 250.
(18) Lipscomb, J. D. *Curr. Opin. Struct. Biol.* **2008**, *18*, 644.
(19) Broderick, J. B. *Essays Biochem.* **1999**, *34*, 173.
(20) Bugg, T. D. H.; Lin, G. *Chem. Commun.* **2001**, *11*, 941.
(21) Somerville, C. C.; Nishino, S. F.; Spain, J. C. *J. Bacteriol.* **1995**, *177*, 3837.
(22) Nishino, S. F.; Spain, J. C. *Appl. Environ. Microbiol.* **1993**, *59*, 2520.
(23) He, Z.; Spain, J. C. *J. Ind. Microbiol. Biotechnol.* **2000**, *25*, 25.
(24) Takenaka, S.; Murakami, S.; Shinke, R.; Hatakeyama, K.; Yukawa, H.; Aoki, K. *J. Biol. Chem.* **1997**, *272*, 14727.
(25) Wu, J.-F.; Sun, C.-W.; Jiang, C.-Y.; Liu, Z.-P.; Liu, S.-J. *Arch. Microbiol.* **2005**, *183*, 1.
(26) Li, D.-F.; Zhang, J.-Y.; Hou, Y.-J.; Liu, L.; Hu, Y.; Liu, S.-J.; Wang, D.-C.; Liu, W. *Acta Crystallogr.* **2013**, *D69*, 32.
(27) Li, X.; Guo, M.; Fan, J.; Tang, W.; Wang, D.; Ge, H.; Rong, H.; Teng, M.; Niu, L.; Liu, Q.; Hao, Q. *Protein Sci.* **2006**, *15*, 761.
(28) Kucharczyk, R.; Zagulski, M.; Rytka, J.; Herbert, C. J. *FEBS Lett.* **1998**, *424*, 127.
(29) Colabroy, K. L.; Zhai, H.; Li, T.; Ge, Y.; Zhang, Y.; Liu, A.; Ealick, S. E.; McLafferty, F. W.; Begley, T. P. *Biochemistry* **2005**, *44*, 7623.
(30) Zhang, Y.; Colabroy, K. L.; Begley, T. P.; Ealick, S. E. *Biochemistry* **2005**, *44*, 7632.
(31) Wu, J.-f.; Jiang, C.-y.; Wang, B.-j.; Ma, Y.-f.; Liu, Z.-p.; Liu, S.-j. *Appl. Environ. Microbiol.* **2006**, *72*, 1759.
(32) Colabroy, K. L.; Begley, T. P. *J. Bacteriol.* **2005**, *187*, 7866.
(33) Colabroy, K. L.; Begley, T. P. *J. Am. Chem. Soc.* **2005**, *127*, 840.
(34) Kurnasov, O.; Goral, V.; Colabroy, K.; Gerdes, S.; Anantha, S.; Osterman, A.; Begley, T. P. *Chem. Biol.* **2003**, *10*, 1195.
(35) Kovaleva, E. G.; Lipscomb, J. D. *Science* **2007**, *316*, 453.
(36) Poddel'sky, A. I.; Cherkasov, V. K.; Abakumov, G. A. *Coord. Chem. Rev.* **2009**, *253*, 291.
(37) Chun, H.; Bill, E.; Bothe, E.; Weyhermüller, T.; Wieghardt, K. *Inorg. Chem.* **2002**, *41*, 5091.
(38) Chun, H.; Verani, C. N.; Chaudhuri, P.; Bothe, E.; Bill, E.; Weyhermüller, T.; Wieghardt, K. *Inorg. Chem.* **2001**, *40*, 4157.
(39) Chun, H.; Weyhermüller, T.; Bill, E.; Wieghardt, K. *Angew. Chem., Int. Ed.* **2001**, *40*, 2489.
(40) Chun, H.; Bill, E.; Weyhermüller, T.; Wieghardt, K. *Inorg. Chem.* **2003**, *42*, 5612.
(41) Min, K. S.; Weyhermüller, T.; Wieghardt, K. *Dalton Trans.* **2003**, 1126.
(42) Mukherjee, S.; Weyhermüller, T.; Bill, E.; Wieghardt, K.; Chaudhuri, P. *Inorg. Chem.* **2005**, *44*, 7099.
(43) Bittner, M. M.; Lindeman, S. V.; Fiedler, A. T. *J. Am. Chem. Soc.* **2012**, *134*, 5460.
(44) Bittner, M. M.; Kraus, D.; Lindeman, S. V.; Popescu, C. V.; Fiedler, A. T. *Chem.—Eur. J.* **2013**, *19*, 9686.
(45) Chakraborty, B.; Paine, T. K. *Angew. Chem., Int. Ed.* **2013**, *52*, 920.
(46) Britovsek, G. J. P.; England, J.; White, A. J. P. *Inorg. Chem.* **2005**, *44*, 8125.
(47) Paria, S.; Halder, P.; Paine, T. K. *Inorg. Chem.* **2010**, *49*, 4518.
(48) *APEX 2, v2.1−0*; Bruker AXS: Madison, WI, 2006.
(49) Sheldrick, G. M. *SHELXL-97, Program for crystal structure refinement;* University of Göttingen: Göttingen, Germany, 1997.
(50) Lee, C.; Yang, W.; Parr, R. G. *Phys. Rev. B* **1988**, *37*, 785.
(51) Becke, A. D. *J. Chem. Phys.* **1993**, *98*, 5648.
(52) Geng, C.; Ye, S.; Neese, F. *Angew. Chem., Int. Ed.* **2010**, *122*, 5853.
(53) Janardanan, D.; Wang, Y.; Schyman, P.; Que, L., Jr.; Shaik, S. *Angew. Chem., Int. Ed.* **2010**, *49*, 3342.
(54) Scepaniak, J. J.; Vogel, C. S.; Khusniyarov, M. M.; Heinemann, F. W.; Meyer, K.; Smith, J. M. *Science* **2011**, *331*, 1049.
(55) McLean, A. D.; Chandler, G. S. *J. Chem. Phys.* **1980**, *72*, 5639.
(56) Dunning, T. H., Jr.; Hay, P. J. In *Modern Theoretical Chemistry;* Schaefer, H. F., Ed.; Plenum: New York, 1976; Vol. *3*, p 1.
(57) Frisch, M. J.; Trucks, G. W.; Schlegel, H. B.; Scuseria, G. E.; Robb, M. A.; Cheeseman, J. R.; Scalmani, G.; Barone, V.; Mennucci, B.; Petersson, G. A.; Nakatsuji, H.; Caricato, M.; Li, X.; Hratchian, H. P.; Izmaylov, A. F.; Bloino, J.; Zheng, G.; Sonnenberg, J. L.; Hada, M.; Ehara, M.; Toyota, K.; Fukuda, R.; Hasegawa, J.; Ishida, M.; Nakajima, T.; Honda, Y.; Kitao, O.; Nakai, H.; Vreven, T.; Montgomery, J. A.; , Jr., Peralta, J. E.; Ogliaro, F.; Bearpark, M.; Heyd, J. J.; Brothers, E.; Kudin, K. N.; Staroverov, V. N.; Kobayashi, R.; Normand, J.; Raghavachari, K.; Rendell, A.; Burant, J. C.; Iyengar, S. S.; Tomasi, J.; Cossi, M.; Rega, N.; Millam, J. M.; Klene, M.; Knox, J. E.; Cross, J. B.; Bakken, V.; Adamo, C.; Jaramillo, J.; Gomperts, R.; Stratmann, R. E.; Yazyev, O.; Austin, A. J.; Cammi, R.; Pomelli, C.; Ochterski, J. W.; Martin, R. L.; Morokuma, K.; Zakrzewski, V. G.; Voth, G. A.; Salvador, P.; Dannenberg, J. J.; Dapprich, S.; Daniels, A. D.; Farkas, O.; Foresman, J. B.; Ortiz, J. V.; Cioslowski, J.; , and Fox, D. J. *Gaussian 09,* Revision A.1; Gaussian, Inc.: Wallingford, CT, 2009.
(58) Barone, V.; Cossi, M. *J. Phys. Chem. A* **1998**, *102*, 1995.
(59) Cossi, M.; Barone, V. *J. Chem. Phys.* **2001**, *115*, 4708.
(60) Cossi, M.; Rega, N.; Scalmani, G.; Barone, V. *J. Comput. Chem.* **2003**, *24*, 669.
(61) Petersson, G. A.; Bennett, A.; Tensfeldt, T. G.; Al-Laham, M. A.; Shirley, W. A.; Mantzaris, J. *J. Chem. Phys.* **1988**, *89*, 2193.
(62) Wertz, D. H. *J. Am. Chem. Soc.* **1980**, *102*, 5316.
(63) Spickermann, C. *Entropies of Condensed Phases and Complex Systems;* Springer Theses: Berlin, 200; Chapter 3.
(64) Malakar, T.; Roy, L.; Paul, A. *Chem.—Eur. J.* **2013**, *19*, 5812.
(65) Li, H.; Wang, X.; Huang, F.; Lu, G.; Jiang, J.; Wang, Z.-X. *Organometallics* **2011**, *30*, 5233.
(66) Liang, Y.; Liu, S.; Xia, Y.; Li, Y.; Yu, Z.-X. *Chem.—Eur. J.* **2008**, *14*, 4361.
(67) Halder, P.; Paria, S.; Paine, T. K. *Chem.—Eur. J.* **2012**, *18*, 11778.
(68) Chiou, Y.-M.; Que, L., Jr. *J. Am. Chem. Soc.* **1995**, *117*, 3999.

(69) Paine, T. K.; Paria, S.; Que, L., Jr. *Chem. Commun.* **2010**, *46*, 1830.
(70) Chiou, Y.-M.; Que, L., Jr. *Inorg. Chem.* **1995**, *34*, 3577.
(71) Suzuki, H.; Furusho, Y.; Higashi, T.; Ohnishi, Y.; Horinouchi, S. *J. Biol. Chem.* **2006**, *281*, 824.
(72) Toussaint, O.; Lerch, K. *Biochemistry* **1987**, *26*, 8567.
(73) Chaudhuri, P.; Verani, C. N.; Bill, E.; Bothe, E.; Weyhermüller, T.; Wieghardt, K. *J. Am. Chem. Soc.* **2001**, *123*, 2213.
(74) Carter, S. M.; Sia, A.; Shaw, M. J.; Heyduk, A. F. *J. Am. Chem. Soc.* **2008**, *130*, 5838.
(75) Weinstock, I. A. *Inorg. Chem.* **2008**, *47*, 404.
(76) Georgiev, V.; Noack, H.; Borowski, T.; Blomberg, M. R. A.; Siegbahn, P. E. M. *J. Phys. Chem. B* **2010**, *114*, 5878.
(77) Chatterjee, S.; Sheet, D.; Paine, T. K. *Chem. Commun.* **2013**, *49*, 10251.
(78) Christian, G. J.; Ye, S.; Neese, F. *Chem. Sci.* **2012**, *3*, 1600.